Thesis for the degree of Doctorate of Engineering

Collisional transport in edge transport barriers and stellarators

Stefan Buller

CHALMERS

Department of Physics
Chalmers University of Technology
Göteborg, Sweden, 2019

Collisional transport in edge transport barriers and stellarators
Stefan Buller
ISBN 978-91-7905-151-8

Doktorsavhandlingar vid Chalmers tekniska högskola
Ny serie nr 4618
ISSN 0346-718X

Department of Physics
Chalmers University of Technology
SE–412 96 Göteborg
Sweden
Telephone +46 (0) 31 772 1000

Some figures in this thesis are in color only in the electronic version, available online through Chalmers Publication Library.

Cover:
An artistic interpretation of collisional transport in a toroidal magnetic field. Colliding billiard balls are a textbook example of a collision.

Printed in Sweden by
Reproservice
Chalmers Tekniska Högskola
Göteborg, Sweden, 2019

Collisional transport in edge transport barriers and stellarators

Stefan Buller
Department of Physics
Chalmers University of Technology

Abstract

Nuclear fusion has the potential to generate abundant and clean energy. In magnetic confinement fusion, the temperatures needed to achieve fusion are obtained by confining a hot plasma with magnetic fields. To maintain these hot temperatures and realize the potential of fusion, an understanding of transport mechanisms of particles and energy in these plasmas is needed. This thesis theoretically investigates two aspects of collisional transport in magnetically confined fusion plasmas: the collisional transport in tokamak transport barriers and of highly-charged impurities in stellarators.

The tokamak and the stellarator are the two most developed solutions to magnetically confining a plasma. Tokamaks frequently operate in a regime (the *H-mode*) with a transport barrier near the edge of the plasma, in which turbulence is spontaneously reduced. This leads to reduced energy and particle transport and sharp temperature and density gradients. These sharp gradients challenge the modeling capabilities based on the conventional theory of collisional transport, which relies on the assumption that the density, temperature, and electrostatic potential of the plasma do not vary strongly over a particle orbit. This thesis explores an extension of the conventional theory that accounts for these effects, by means of numerical simulations.

Another limit that challenges the conventional assumptions is when the density of an impurity varies along the magnetic field. This happens for heavy impurities, such as iron or tungsten, which can enter the plasma from interactions with the walls of the reactor. Due to their high charge, these impurities are sensitive to even slight variations in electrostatic potential in the plasma, which causes their density to vary along the magnetic field. This density variation can qualitatively affect how the impurities are transported. This is explored in the latter half of this thesis, with an eye towards how this effect could be used to prevent impurities from accumulating in the core of stellarators, where they are detrimental.

Keywords: fusion, plasma physics, transport, collisional transport, impurity transport, pedestal, tokamak, stellarator

Publications

[A] I. Pusztai, S. Buller, and M. Landreman, *Global effects on neoclassical transport in the pedestal with impurities*, Plasma Physics and Controlled Fusion **58**, 085001 (2016).
https://doi.org/10.1088/0741-3335/58/8/085001

[B] S. Buller, I. Pusztai, S.L. Newton, and J.T. Omotani, *Neoclassical flows in deuterium-helium plasma density pedestals*, Plasma Physics and Controlled Fusion **59**, 055019 (2017).
https://doi.org/10.1088/1361-6587/aa658a

[C] S. Buller and I. Pusztai, *Isotope and density profile effects on pedestal neoclassical transport*, Plasma Physics and Controlled Fusion **59**, 105003 (2017).
https://doi.org/10.1088/1361-6587/aa7e5c

[D] S. Buller, H.M. Smith, P. Helander, A. Mollén, S.L. Newton, and I. Pusztai, *Collisional transport of impurities with flux-surface varying density in stellarators*, Journal of Plasma Physics **84** 905840409 (2018).
https://doi.org/10.1017/S0022377818000867

[E] S. Buller, H.M. Smith, A. Mollén, S.L. Newton, and I. Pusztai, *Optimization of flux-surface density variation in stellarator plasmas with respect to the transport of collisional impurities*, Nuclear Fusion **59** 066028 (2019).
https://dx.doi.org/10.1088/1741-4326/ab12a7

[F] S. Buller, H.M. Smith, A. Mollén, S.L. Newton, and I. Pusztai, *The importance of the classical channel in the impurity transport of optimized stellarators*, Journal of Plasma Physics **85** 175850401 (2019).
https://doi.org/10.1017/S002237781900045X

Statement of contribution

Paper A I performed the simulations, produced the figures, and was involved in writting the text.

Paper B I performed the simulations, produced the figures, and wrote most of the text with input from coauthors. I extended the PERFECT code to allow for momentum sources.

Paper C I performed the simulations, produced the figures, and wrote most of the text, with input from coauthors.

Paper D I performed the analytical calculations, with help from coauthors. The computer implementation of the resulting semi-analytical expressions uses scripts by H.M. Smith. I produced the figures and wrote most of the text, with input from coauthors.

Paper E I extended the scripts by H.M. Smith to numerically implement the expression for the transport of non-trace impurities from Paper D. I ran the optimization algorithms to calculate optimal impurity density variations. I produced the figures and wrote most of the text, with input from coauthors.

Paper F I performed the analytical calculations, with input from coauthors. I ran the SFINCS simulations for the left column of figure 2. I produced all the figures and wrote most of the text with input from coauthors.

Acknowledgments

A number of people have been instrumental in shaping this thesis:

Nothing in this thesis would have been the same without the help and supervision of István Pusztai, who has always been willing to answer my questions and enter into deep discussions. István has a great gift for intuitively explaining plasma transport, and has greatly shaped my thinking about the content of this thesis.

My co-supervisors John Omotani and Sarah Newton, who have guided me into the world of physics codes and physics.

Throughout my PhD studies, I've had the pleasure of working with many talented people. Thanks to Matt Landreman, Per Helander, Håkan Smith, and Albert Mollén for their company and contributions to this thesis. Also thanks to Carine Giroud for her help with obtaining JET data.

Last but not least, I would like to thank the members of the Chalmers Plasma Theory group (past and present) for creating a warm and welcoming work environment, making it a pleasure to work with plasma physics. A special thanks to Tünde Fülöp for looking out for us all.

Contents

Abstract iii

Publications iv

Acknowledgements vi

Contents viii

1 Introduction 1
- 1.1 The high-confinement mode . . . 4
- 1.2 Transport of highly-charged impurities in stellarators . . . 7
- 1.3 Thesis outline . . . 8

2 Basics of magnetic confinement 9
- 2.1 Magnetic confinement of a single particle . . . 10
  - 2.1.1 Nearly-constant magnetic fields . . . 12
  - 2.1.2 Magnetic fields for confinement . . . 15
- 2.2 Kinetic theory and collision operators . . . 22
  - 2.2.1 Transport moments . . . 26
- 2.3 The drift-kinetic equation . . . 28
  - 2.3.1 Approximations and ordering assumptions . . . 29
  - 2.3.2 Hazeltine's recursive drift-kinetic equation . . . 31
  - 2.3.3 Transport moments revisited . . . 34

3 Transport in tokamak pedestals 37
- 3.1 Linear drift-kinetic equation for tokamak pedestals . . . 37
- 3.2 Moment equations for the pedestal . . . 42
- 3.3 The PERFECT code . . . 45

4 Transport of highly-charged impurities **49**
4.1 Highly-charged impurities 50
4.2 The **SFINCS** code 55

5 Summary of papers **57**

References **65**

Chapter 1

Introduction

As energy is conserved, every process – such as reading this text or even thinking – can be thought of as converting energy from one form to another. However, when energy is transferred within a system, it is typically redistributed over more parts of the system, until it is so thinly distributed that it can no longer be used to perform work. This result – the second law of thermodynamics – implies that useful energy ("free energy") is effectively consumed, and cannot be produced [1, 2].

Although we cannot create energy, we can extract it from systems which have yet to reach their minimum free energy state. The most prominent everyday example of such a system is the Sun, which effectively acts as a battery for the entire solar system.

The source of the Sun's energy lies in the curious fact that the nuclear binding energy per nucleon increases with mass for light atomic nuclei, so that energy can be extracted by merging lighter elements together – the process of *nuclear fusion*. The binding energy continues to increase until around ^{62}Ni, which is therefore the heaviest element that can be formed with a net energy gain [3–5]. Since roughly 75% (by mass) of the ordinary matter in the universe is hydrogen [6], it would seem that a vast amount of energy could potentially be extracted by fusion. However, the fact that the universe *is* mostly hydrogen also tells us that fusion does not happen easily: These nuclei have been firmly stuck in local free energy minima since the early eras of our universe.

The difficulty lies in the fact that atomic nuclei repel each other, so their energetically favorable union can only occur if their kinetic energy is sufficiently high to overcome the Coulomb barrier between them. To put things in perspective, a thermal particle at room temperature has

a kinetic energy around 25 meV, while an energy of about 0.1 MeV is required to take advantage of the maximum cross section of the fusion reaction between deuterium and tritium isotopes [7, 8], the deuterium-tritium (D-T) reaction[1].

Despite the high energies required, fusion is regularly achieved in nuclear physics experiments with ion beams [9]. However, these experimental setups cannot be utilized as an energy technology. The fundamental problem is that beams thermalize due to Coulomb interactions at a much higher rate than fusion reactions occur, so that the kinetic energy of the beam thermalizes before a significant amount of fusion reactions can take place.

To counter such problems, the ions must be prevented from rapidly leaving the system, and must be energetic enough that their thermalized velocity distribution has a sufficiently large number of ions with high enough energies to achieve fusion. For terrestrial fusion, temperatures around one hundred million Kelvin are required [10], which is about 10 times hotter than the core of the Sun [11].

An attractive way to confine such a hot, ionized gas is to utilize magnetic fields – an approach known as *magnetic confinement fusion*. An ionized gas under these conditions is called a (magnetized) *plasma*. A plasma is a gas of charged particles which is dominated by collective – rather than single particle – effects. A plasma is said to be *magnetized* when the magnetic field is strong enough to dominate the particle dynamics, which essentially is a requirement for magnetic confinement.

When the plasma is confined, the fusion reactions themselves can potentially be used to maintain the temperature of the plasma. Consider the D-T reaction,

$$D + T \rightarrow {}^4\mathrm{He} + n + 17.6\,\mathrm{MeV}, \tag{1.1}$$

where energy and momentum conservation demands that 1/5 of the released energy (3.5 MeV) goes to the helium ion ^{4}He, and 4/5 (14.1 MeV) to the neutron n. Since the helium ions are charged, they will also be confined by the magnetic field, and can transfer their kinetic energy to the fuel. If the heating generated in this way is sufficiently large to compensate for the net energy flux leaving the fusing plasma, it can sustain itself for as long as it is refueled. The viability of a fusion power plant

[1] This is the least difficult fusion reaction to extract energy from on Earth, due to the large amount of energy released in the reaction, its high fusion cross-section at relatively "low" energies, and the abundance of fuel.

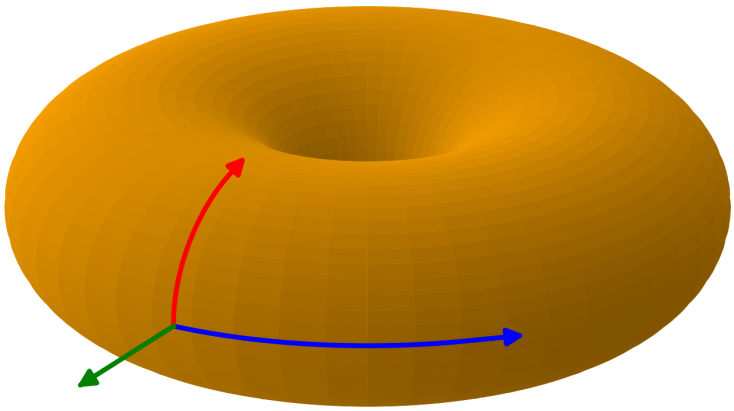

Figure 1.1: An illustration of the three directions in a toroidal coordinate system: The blue arrow indicates the toroidal direction, the red arrow the poloidal direction, and the green arrow the radial direction.

thus depends on achieving low energy losses, and hence we need a solid understanding of these losses in order to design and predict the behavior of such power plants.

One of the most promising magnetic confinement schemes for a fusion reactor is the *tokamak*. The tokamak possesses an axisymmetric magnetic field in the shape of nested toruses, with a large externally generated magnetic field in the long direction around the torus (in the *toroidal direction*, blue in Figure 1.1); and a smaller field along the short direction around the torus (the poloidal direction, red in Figure 1.1), generated by currents in the plasma.

The first part of this thesis is concerned with modeling of the transport of heat, particles, and momentum in tokamak fusion plasmas. Specifically, we are interested in transport in a sharp gradient region that is sometimes found near the edge of tokamaks. These *edge transport barriers*, and the operating regime in which they appear, are described further in Section 1.1.

Another scheme for achieving magnetic confinement is the *stellarator*, which has a less restricted geometry than the tokamak in the sense of not possessing toroidal symmetry. This makes it possible to generate the confining magnetic fields without driving a current in the plasma [12] – which is an advantage for steady-state reactor operation, and for avoiding current-driven instabilities [13] and runaway electron generation [14].

The main downside is that the lack of symmetry makes these devices complicated to design and build. Relevant for this thesis is that the lack of symmetry causes the transport in the plasma to become sensitive to inward electric fields [15]. These inward fields are expected at fusion relevant conditions [16, 17], and can pull impurities into the center of the plasma [15], which makes impurity accumulation especially troublesome for stellarators.

Impurities are non-fuel ions that can enter the plasma in various ways, for example through erosion of the wall of the reactor due to energy flux from the plasma. While any charged particle in a plasma will emit energy in the form of radiation, impurities radiate much more strongly than the hydrogen fuel due to their high charge. The walls of a fusion reactor will likely have to be made out of heat-resistant materials like tungsten (proton number 74) [18], which cannot be allowed to accumulate in the middle of the hot plasma.

The tokamak and the stellarator are introduced in more detail at the end of Chapter 2; in the two following sections, we first outline relevant details of the edge transport barrier in tokamaks, and introduce the problem of calculating the transport of highly-charged impurities in stellarators.

1.1 The high-confinement mode

In order to achieve the hundred million Kelvin required in a magnetic fusion reactor on our cold planet, large temperature gradients need to be maintained. With larger gradients, the reactor can be made smaller and thus more economically attractive.

However, temperature gradients are sources of free energy, and naturally decay unless heating is provided. The rate at which this decay happens typically increases with the gradients. Large steady-state gradients thus either require large applied heating, or that the heat flux driven by a given gradient is somehow made small (roughly speaking, the heat diffusivity should be lowered). The former option is unattractive for a reactor, which should therefore be designed to minimize the heat transport.

Unfortunately, the heat transport in modern fusion experiments is frequently observed to be *stiff*, i.e., it increases rapidly once the gradient crosses some threshold known as a *critical gradient* [19–21]. The origin of this increase in transport can be attributed to the excitation of

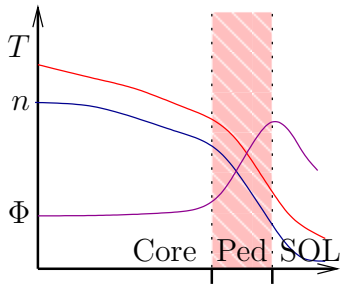

Figure 1.2: An illustration of radial profiles of temperature T, density n and electrostatic potential Φ in the edge of an H-mode tokamak plasma, with the core, pedestal ("Ped"), and Scrape-Off layer ("SOL") regions highlighted. See the text for an explaination of the different regions.

small-scale turbulent structures, which give rise to a sizable turbulent transport [22]. This turbulent transport effectively limits the gradients to the critical values, which thus implies a minimum size for a plasma with fusion relevant temperatures.

As larger reactors imply a larger capital cost, understanding and suppressing plasma turbulence would be a major step towards economically viable fusion power. In fact, turbulence is routinely suppressed in so-called *edge transport barriers*, in fusion devices operated in the *high-confinement mode* [23, 24], often called simply the *H-mode*. The reduction in turbulent transport allows for sharp gradients to develop in the edge of these H-mode plasmas, a feature known as the *pedestal* [25]. This is illustrated in Figure 1.2, which schematically shows radial profiles of temperature (T), density (n), and the electrostatic potential (Φ) in the edge of an H-mode tokamak plasma, with different radial regions highlighted.

The sharp gradients in the pedestal will likely be useful for future fusion reactors: All current plans for magnetic fusion reactors feature at least an edge transport barrier [26, 27], and sometimes additional internal transport barriers [26]. Transport barriers are also interesting to study theoretically, as the sharper gradients challenge some of the assumptions typically used to study transport in fusion plasmas. In the context of the core and pedestal transport, these assumptions may be stated as follows:

In the core region, the radial transport is predominantly turbulent and the gradients are thus limited. In this region the plasma profiles

vary weakly over a particle orbit and over the typical size of coherent turbulent structures, which means that the transport can be described by a conventional *radially local* theory, in which the transport at a given radius can be described in terms of plasma parameters at that radius.

The typical arguments used to derive a local theory can be sketched as follows: Confined particle orbits in tokamak magnetic fields are typically close to periodic. If a particle moves very little radially during its approximately periodic orbit, we can average over multiple periods to obtain an effective force acting at the average radial location of the particle, r. To illustrate this, we expand a plasma profile X around r

$$X(r+\Delta r) = X(r) + \Delta r \left.\frac{\partial X}{\partial r}\right|_r + \mathcal{O}\left(\Delta r^2\right), \tag{1.2}$$

where Δr is the difference between r and the actual radial position of the particle. If the second term is small, $\Delta r \left.\frac{\partial X}{\partial r}\right|_r \ll X(r)$, only a low order approximation to Δr will be needed, so that we can approximate $X(r+\Delta r) \approx X(r)$ for the purpose of calculating Δr itself. This approximation yields a *radially local* description of the plasma, as the X felt by the particle over its orbit (1.2) can be expressed entirely in terms of the value and derivative(s) of X at r.

On the other hand, in the pedestal region ("Ped" in Figure 1.2), the profiles can vary significantly over an orbit width, so that the derivative terms in (1.2) will not be small, and a local theory is not valid. This complicates the understanding of the H-mode, as the transport at a given radius r does not only depend on the plasma properties at r: the transport is *radially global*.

Due to the radially global nature of the pedestal transport, it will also be affected by the outermost region depicted in Figure 1.2, the *scrape-off layer* ("SOL"). This is a comparatively sparse region located outside the confined region. Here, the magnetic field connects directly to the wall, so plasma is no longer confined. This region will not be treated in this thesis, but ought to be included in more complete pedestal models.

In general, the modeling presented in the tokamak pedestal part of this thesis is not meant to be predictive of pedestal transport, as accounting for all the relevant processes (collisional and turbulent transport, instabilities, SOL physics – such as wall-plasma interactions, etc.) in a radially global setting is both conceptually and computationally extremely difficult. Instead, we study the reduced problem of collisional transport in a sharp gradient region, which is theoretically interesting as a simple model for investigating global effects, and experimentally

relevant, as the pedestal transport is often found to be comparable to predictions of naive, radially local collisional transport models [28–32].

1.2 Transport of highly-charged impurities in stellarators

The second topic of this thesis is on the transport of highly-charged impurities in stellarator plasmas. Any charged particle in a plasma will radiate energy, and it is thus useful from an energy balance point of view to minimize the presence of non-fuel ions. Since the emitted radiation scales strongly with charge [33], the problem becomes much more severe for highly-charged impurities. At worst, the strong cooling due to impurities may cause the plasma to disrupt by driving thermal instabilities.

Although their high charge makes these impurities a threat to energy confinement, it also means that they interact more strongly among themselves and with other species in the plasma through Coulomb collisions. This is beneficial from a modelling point of view, as it causes the impurities to quickly reach a local thermodynamic equilibrium, which means that their velocity distribution will be very close to a Maxwellian.

On the other hand, the high charge of the impurities also makes them susceptible to slight variations in the electrostatic potential. Normally in a fusion plasma, most of the particles are free to move along the magnetic field uninhibited, and thus any significant variation in the electrostatic potential would quickly be evened out. This cancellation will however not be exact, as there are forces beside the electric force acting on the particles – such as collisional friction or the magnetic mirror force (to be discussed in Chapter 2). As these other forces typically are small, the uncancelled electrostatic potential variation will also be small, and only highly-charged particles will be sensitive to these variations. This picture applies to both tokamaks and stellarators, and is known to affect the transport of impurities in tokamaks [34, 35]. Only recently has this effect been studied for stellarators [36], where it was hoped that the effect could explain the absence of impurities in so called *impurity hole* discharges in the Japanese stellarator LHD (Large Helical Device). While this effect does not appear to be able to explain the impurity hole, it nevertheless has been found to have a large effect on the impurity transport in the scenarios where it has been investigated [36, 37].

The effect of flux-surface variation of the potential is of potential interest, not only to increase the predictive power of impurity transport

modelling, but also for the development of methods to control impurities: The electrostatic potential variation can be affected by tailoring the plasma heating [38], which thus provides a potential method for affecting the impurity transport. Chapter 4 describes a derivation of a semi-analytic expression for the collisional transport of impurities, which may be useful for optimizing the plasma heating so that impurities are not accumulated in the plasma, and can be useful for calculating bounds on collisional impurity transport if the potential variations are not measured or controlled.

1.3 Thesis outline

The rest of this thesis is structured as follows. The upcoming chapters present the concepts needed to understand the work done as part of this thesis, the unifying theme being collisional transport.

In Chapter 2, we introduce the basic concepts needed to describe how to confine plasmas with magnetic fields, starting with single-particle motion, proceeding through the kinetic equation, and finally ending with the drift-kinetic equation. In Chapter 3 and Chapter 4, we simplify the drift-kinetic equation in the limits of large gradients or large impurity charge. These are the limits of interest to describe the distribution function in the pedestal of tokamaks, and the transport of heavy impurities in a stellarator, respectively. In the final chapter, Chapter 5, we summarize the results obtained using these equations; these results are presented in detail in the included papers.

Chapter 2

Basics of magnetic confinement

In this chapter, we describe the basic concepts underlying most of magnetic fusion research, including the work done in this thesis. We start by describing single particle orbits in constant magnetic fields, which provides a simple example of how magnetic fields can be used to confine a particle. In this context, we introduce the concept of the guiding-center, which is then used to derive approximate solutions to the equations of motion in more general fields, allowing us to address the shortcomings of the constant field scenario and fully confine a particle. We then discuss how a particle is confined in the toroidal fields used in tokamaks and stellarators, which is one of the central results needed as a background to understand this thesis.

To describe a plasma – rather than just a single particle – the interactions between the plasma particles also need to be taken into account. In Section 2.2, we sketch a statistical approach for describing the evolution of a distribution of N-particles interacting via long-range Coulomb collisions and macroscopic electromagnetic fields, resulting in the Fokker-Planck equation that is fundamental to most kinetic descriptions of plasma.

The particle distribution function can then be used to calculate particle, heat and momentum fluxes, which are the quantities needed to evaluate the quality of our magnetic confinement system in the presence of collisions. These calculations would most generally involve solving the Fokker-Planck equation, which is often difficult. By combining the Fokker-Planck equation with the results of single particle motion de-

rived in this chapter, we simplify the Fokker-Planck equation, yielding the drift-kinetic equation, which is the starting point for most theoretical studies of collisional transport in magnetized plasmas.

2.1 Magnetic confinement of a single particle

Magnetic confinement relies on the Lorentz-force to confine charged particles,

$$\boldsymbol{F} = Ze(\boldsymbol{E} + \boldsymbol{v} \times \boldsymbol{B}), \tag{2.1}$$

where $\boldsymbol{F}$ is the force acting on a particle with charge Ze, where e is the elementary charge; $\boldsymbol{v}$ is the particle velocity, $\boldsymbol{E}$ is the electric field, and $\boldsymbol{B}$ is the magnetic field. In general, the fields depend on position and time – although we will not consider time variations in this thesis. In addition, the charged particles themselves generate electromagnetic fields, which couple the dynamics of different particles and greatly complicate the problem.

As a starting point, we first consider the motion of a single particle in a stationary, homogeneous $\boldsymbol{B}$ with $\boldsymbol{E} = 0$. In the direction perpendicular to the field (which we denote by a subscript $\perp$), the particle will circle a magnetic field-line with a radius given by the gyroradius $\rho = v_\perp/\Omega$, where $\Omega = ZeB/m$ is the gyrofrequency, m the particle mass, and $v_\perp$ its velocity perpendicular to the magnetic field. Specifically, the perpendicular motion is given by

$$\boldsymbol{x}_\perp = \boldsymbol{X}_\perp + \boldsymbol{\rho}, \tag{2.2}$$

$$\boldsymbol{v}_\perp = v_\perp[\boldsymbol{e}_1 \cos(\Omega t) - \boldsymbol{e}_2 \sin(\Omega t)] \equiv v_1 \boldsymbol{e}_1 + v_2 \boldsymbol{e}_2, \tag{2.3}$$

where $\boldsymbol{e}_1, \boldsymbol{e}_2$ are unit-vectors that form an orthonormal basis together with $\boldsymbol{b}$, which is the unit vector in the $\boldsymbol{B}$ direction; $\boldsymbol{X}_\perp$ is a constant vector that gives the position of the center of gyration in the plane perpendicular to $\boldsymbol{B}$. The gyro-radius vector, $\boldsymbol{\rho}$, is the time-integral of $\boldsymbol{v}_\perp$, and can thus be written

$$\boldsymbol{\rho} = \rho[\boldsymbol{e}_1 \sin(\Omega t) + \boldsymbol{e}_2 \cos(\Omega t)] = \frac{\boldsymbol{b} \times \boldsymbol{v}_\perp}{\Omega}. \tag{2.4}$$

As time evolves, only the *gyrophase*,

$$\gamma = \Omega t = -\arctan \frac{v_2}{v_1}, \tag{2.5}$$

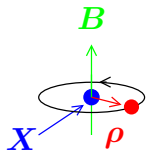

Figure 2.1: The movement of a charged particle (red dot) in a constant magnetic field $\boldsymbol{B}$, where $\boldsymbol{X}$ denotes the position of the center of gyration (blue dot), and $\boldsymbol{\rho}$ is the gyroradius-vector.

changes, and the particle is thus confined within a radius ρ in the direction perpendicular to the magnetic field. This is the basis of magnetic confinement, and is illustrated in Figure 2.1.

However, in the direction parallel to the magnetic field (which we denote by a subscript $\|$), the particle moves with a constant velocity, $v_\|$, and is thus not confined to a finite region.

If we introduce a constant force $\boldsymbol{F}$ in the constant magnetic field case – due to, for example, a constant electric field – the particle will accelerate indefinitely due to any component of $\boldsymbol{F}$ parallel to $\boldsymbol{B}$. Any perpendicular component $\boldsymbol{F}_\perp$ will cause the particle to execute an additional *drift motion* perpendicular to the magnetic field

$$\boldsymbol{v}_\mathrm{d} = \frac{\boldsymbol{F} \times \boldsymbol{B}}{ZeB^2}. \tag{2.6}$$

Hence the addition of a constant $\boldsymbol{F}$ causes the particle to drift away from a given field-line.

The above discussion suggests that an infinite, straight magnetic field with no external forces can confine a particle. Unfortunately, such a configuration is not practically realizable, and we thus have to consider more general fields.

To prepare for the discussion of more general fields, we devote the remainder of this section to introducing the concept of the *guiding-center*. In magnetic fusion, it is often convenient to consider the position of the center of the gyrating motion – the guiding-center – rather than the particle position. There are numerous reasons for this: As shown in the following section, it will allow us to construct approximate analytical solutions for the motion in more general fields that remains accurate over times much longer than $1/\Omega$ [39, 40]. In simulations of particle orbits, it alleviates the burden of having to resolve the short time and

length-scales associated with the gyromotion. Finally, in kinetic theory, it allows for the elimination of the gyrophase γ as a phase-space coordinate, which reduces the dimensionality of the problem [41] – a result that we will demonstrate in Section 2.3.

As suggested by the notation in (2.2), we denote the guiding center position by $\boldsymbol{X}$. We define the *gyroaverage* of a quantity A as

$$\langle A \rangle_{\boldsymbol{X}} = \frac{1}{2\pi} \oint \mathrm{d}\gamma A(\boldsymbol{X}, v_\parallel, v_\perp, \gamma), \tag{2.7}$$

where $\boldsymbol{X}$, $v_\parallel$ and $v_\perp$ are kept fixed during the average. For the constant magnetic field case, this is equivalent to performing an average over a period of the perpendicular motion. From this definition, it follows that $\langle \boldsymbol{\rho} \rangle_{\boldsymbol{X}} = 0$, $\langle \boldsymbol{v}_\perp \rangle_{\boldsymbol{X}} = 0$, and $\langle \boldsymbol{x} \rangle_{\boldsymbol{X}} = \boldsymbol{X}$. The velocity of the guiding-center is given by $\dot{\boldsymbol{X}} = v_\parallel \boldsymbol{b} + \boldsymbol{v}_\mathrm{d}$, with $\boldsymbol{v}_\mathrm{d}$ given by (2.6) – again reflecting the fact that constant fields will not confine particles in the presence of external forces. Having rephrased this result in terms of the guiding-center, we are now ready to move on to considering magnetic fields with spatial variations.

Of particular interest are magnetic fields with weak variations over the spatial and temporal scales of the gyration, as this class of fields turns out to be sufficiently general to confine particles, and can be treated perturbatively in a manner that yields analytic solutions to the particle motion that remain accurate over reactor relevant time-scales. We consider single-particle motion in such fields in the following section.

2.1.1 Nearly-constant magnetic fields

If we assume that the magnetic field felt by the particle changes little during a gyration, we can view this change as a small perturbation to the constant field case, and use perturbation theory to calculate corrections to the motion in the constant field.

To see this, we expand the magnetic field around the guiding-center $\boldsymbol{X}$:

$$\boldsymbol{B}(\boldsymbol{x}) = \boldsymbol{B}(\boldsymbol{X} + \boldsymbol{\rho}) = \boldsymbol{B}(\boldsymbol{X}) + \boldsymbol{\rho} \cdot \nabla \boldsymbol{B}(\boldsymbol{X}) + \mathcal{O}\left(\rho^2\right). \tag{2.8}$$

Here, we take $\boldsymbol{x} = \boldsymbol{X} + \boldsymbol{\rho}$, which is only exact in the constant field case, but is sufficient for our present purposes, as we will see[1].

[1] For deriving the equation of guiding-center motion accurate to arbitrary order, see e.g. Refs. [42, 43].

If the magnetic field changes little on the gyroradius scale, in the sense that the magnitude of the gradient term in (2.8) is much smaller than the first term, we can view it as giving a small correction to the force acting on the particle. The ratio between the magnitude of the first and second terms in (2.8) is of the order of $\epsilon \equiv \rho|\nabla B|/B$, which will be treated as the small parameter in our perturbation expansion, $\epsilon \ll 1$. For a thermal ion in a typical fusion reactor, $\epsilon \sim 10^{-3}$, which justifies the above treatment.

To lowest order in ϵ, the particle experiences the force due to a constant magnetic field $\boldsymbol{B} = \boldsymbol{B}(\boldsymbol{X})$, so the lowest order motion of the particle is given by a constant motion along the field line and a gyration around the field line, as obtained in the previous section. This is the unperturbed motion.

Using the unperturbed solution, we can calculate corrections to the particle motion perturbatively. The magnetic field felt by the particle along its unperturbed trajectory, is given by the terms written out in (2.8), which hence are sufficient to calculate the motion to order ϵ.

A subtle issue arises from the fact that we need our approximate particle orbit to be valid for many gyrations. The theory of nearly-periodic systems [39] tells us that we obtain a perturbative description of the motion, which is valid for much longer than the gyroperiod, if we average the velocity and force felt by the particle over the unperturbed periodic orbit, and treat these averages as giving an effective velocity and acceleration of the center of the periodic orbit. In the context of nearly-constant magnetic fields, this procedure yields an equation of motion where the guiding-center responds to the average force felt by the particle over its gyro-orbit [39].

The effective gyroaveraged force felt by the guiding-center due to the first order term in (2.8) is

$$\boldsymbol{F}_{\text{eff}} = \langle Ze\boldsymbol{v} \times (\boldsymbol{\rho} \cdot \nabla \boldsymbol{B}(\boldsymbol{X})) \rangle_{\boldsymbol{X}} . \tag{2.9}$$

Evaluating this integral gives

$$\boldsymbol{F}_{\text{eff}} = -mv_{\parallel}^2 \boldsymbol{\kappa} - \mu \nabla B, \tag{2.10}$$

where $\boldsymbol{\kappa} = -\boldsymbol{b} \times (\nabla \times \boldsymbol{b}) = \boldsymbol{b} \cdot \nabla \boldsymbol{b}$ is the curvature of $\boldsymbol{B}$; $\mu = mv_{\perp}^2/(2B)$ is the magnetic moment. Note that here the fields are evaluated at $\boldsymbol{X}$. The two contributions to the effective force can be interpreted physically as follows: The curvature term can be understood as a centrifugal force due to the local radius of curvature of the magnetic field. The second term

can be recognized as the force acting on a current ring with magnetic moment μ.

The fact that the motion of the guiding-center remains accurate over many gyrations is closely related to the concept of *adiabatic invariance* [44, 45]. When formulated in a Lagrangian framework, the independence of the gyroaveraged Lagrangian with respect to γ can be used to derive an invariant [46]. This is an adiabatic invariant if it remains approximately constant over long times, even when a small perturbation is added to the averaged system, i.e. the contribution of the small perturbation does not accumulate. Kruskal [39] has shown that for a Hamiltonian system with only periodic solutions, the Poincaré invariant [47] of the unperturbed system over its period becomes an adiabatic invariant. For the perpendicular motion in a constant magnetic field, this invariant is the magnetic moment μ [45].

Since μ is an adiabatic invariant, it can be viewed as an internal property of the guiding-center, analogous to a particle's spin. Since the particle's kinetic energy can be written as $mv_\parallel^2/2 + \mu B$, we can consider $U = \mu B$ as a contribution to an effective potential energy of the guiding center. From this potential, we can calculate a force $\boldsymbol{F} = -\nabla U$, which gives an intuitive derivation of the second term in (2.10). This term is known as the *mirror force*, as it reflects particles that have insufficient parallel velocities to overcome the effective potential.

Given the effective force (2.10), a drift-velocity $\boldsymbol{v}_\mathrm{d}$ may be calculated from (2.6). If we now let $\boldsymbol{E} \neq 0$ and assume that $\boldsymbol{E}$ is also nearly constant over the particle orbit in the same manner as $\boldsymbol{B}$, the total velocity of the guiding-center becomes

$$\dot{\boldsymbol{X}} = v_\parallel \boldsymbol{b} + \boldsymbol{v}_\mathrm{d}, \tag{2.11}$$

where $v_\parallel$ evolves according to the parallel component of $\boldsymbol{F} = Ze\boldsymbol{E} + \boldsymbol{F}_\mathrm{eff}$ and the drift-velocity $\boldsymbol{v}_\mathrm{d}$ is calculated from $\boldsymbol{F}$ according to (2.6),

$$\boldsymbol{v}_\mathrm{d} = \frac{\boldsymbol{E} \times \boldsymbol{B}}{B^2} + \frac{v_\perp^2}{2\Omega} \boldsymbol{b} \times \nabla \log B + \frac{v_\parallel^2}{\Omega} \boldsymbol{b} \times \boldsymbol{\kappa}. \tag{2.12}$$

The first term is the $\boldsymbol{E} \times \boldsymbol{B}$ drift, while the last two terms in (2.12) are the *magnetic drifts* associated with the effective force (2.10). The magnetic drifts are small in ϵ compared to $v_\perp$, since we assume weakly varying fields, while the $\boldsymbol{E} \times \boldsymbol{B}$ drift in principle can be large. However, the $\boldsymbol{E} \times \boldsymbol{B}$ drifts are usually small compared to the typical velocities

of hydrogen ions or electrons in modern magnetic confinement systems[2] [42], so we assume that the $\boldsymbol{E} \times \boldsymbol{B}$ drift is also small in ϵ, and hence the drift motion corresponds to a small correction to the parallel motion.

Although the drift is small in comparison to the motion parallel to the field line, it must be accounted for to confine particles on reactor-relevant time-scales. In the following section, we explore magnetic field configurations capable of confining the drift-motion of the guiding centers.

2.1.2 Magnetic fields for confinement

In the previous sections, we saw that magnetic fields confine particles in the perpendicular direction, but field inhomogeneities result in a perpendicular drift $\boldsymbol{v}_\mathrm{d}$. In addition, the particle is not confined in the parallel direction.

There are two approaches for remedying the lack of confinement in the parallel direction: One is to have a straight magnetic field of finite extent, where the field crosses a material surface. Such systems are known as *open systems*, since particles traveling along magnetic field-lines have open trajectories which leave the system by hitting the wall. To prevent this, the magnetic field strength can be modulated along the magnetic field-line, so that the mirror force traps particles in low field regions away from the walls. Machines based on this principle are known as *mirror machines*, and remain an active area of research [49]. A more successful approach to fusion energy uses a second method, in which the magnetic field itself is confined to a bounded region, without intersecting any material surfaces. Such systems are known as *closed systems*, since particles traveling along the field-lines remain in the system. For the magnetic field to not vanish at any point on the boundary of this region, the Poincaré-Hopf theorem states that the boundary has to be topologically equivalent to a torus [50, 51]. This thesis is concerned with closed toroidal systems, and the rest of this section describes the requirements on toroidal systems to confine the drifting guiding-centers.

We will start by considering the simplest toroidal configuration, which is a purely toroidal field, for example the field around a wire with cur-

[2] There are exceptions to this, such as Spherical Tokamaks [48] and potentially the pedestal, although we will take a different approach to modeling the electric field in the pedestal in this thesis, see Chapter 3. Also, since the $E \times B$ velocity is the same for all species, it may be comparable to the thermal speed for heavy impurities, which are notably slower than the hydrogen isotopes.

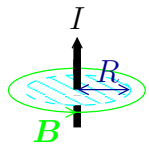

Figure 2.2: An illustration of a purely toroidal magnetic field, generated by a current I flowing in a restricted region of space, such as a wire.

rent, see Figure 2.2. Such a field does *not* confine the *drift orbits* of the guiding centers, but illustrates how these deficiencies can be overcome, which allows us to formulate general requirements for a confining toroidal magnetic field.

Lack of magnetic confinement in a purely toroidal field

To describe a toroidal geometry, we introduce a cylindrical coordinate system, $\{Z, R, \varphi\}$, see Figure 2.3. The radial coordinate R describes the distance from the axis of symmetry, Z is a distance along the axis of symmetry, φ is the azimuthal angle. We also define a toroidal coordinate system $\{\zeta, r, \theta\}$ where r is a distance along the minor radius of the torus, θ is a poloidal angle, and $\zeta = -\varphi$ is known as the toroidal angle in this context – it is defined with the opposite sign of φ to make the toroidal coordinate system right-handed.

We first consider a purely toroidal magnetic field, $\boldsymbol{B} = B\hat{\zeta}$. From symmetry consideration and Ampère's law, the field strength must have the form

$$B = \frac{\mu_0 I}{2\pi R}, \tag{2.13}$$

where I is the current flowing through an imagined circle of radius R centered around the origin. This situation is illustrated in Figure 2.2. In a radial region where I is independent of R, the magnetic field thus decays as $B \propto R^{-1}$.

We now seek to calculate a particle's orbit in the magnetic field (2.13). If B is sufficiently large, so that the gyroradius $\rho(R)$ for a particle at R is much smaller than R, the above field can be approximated as nearly-constant for the purpose of calculating the particle's orbit, and guiding center theory applies. The effective force on the guiding center

(2.10) then becomes

$$\boldsymbol{F}_{\text{eff}} = \left(\frac{m v_{\parallel}^2}{R} + \mu \frac{B}{R} \right) \hat{R} \tag{2.14}$$

which results in the drift

$$\boldsymbol{v}_{\text{d}} = \left(v_{\parallel}^2 + \frac{v_{\perp}^2}{2} \right) \frac{m}{ZeB} \frac{\hat{z}}{R}. \tag{2.15}$$

For $v_{\parallel} \sim v_{\perp}$, the above drift will be small in $\epsilon = \rho/R$, and the guiding center follows the magnetic field to zeroth order in ϵ. As this zeroth-order motion now again is periodic, we can again apply the theory of nearly-periodic motion to derive an effective velocity and force on the center of the drift orbit. If these averages were zero, the drift orbit would be trivially confined, and we would have achieved confinement. Clearly, the purely toroidal field does not achieve this, as the drift experienced by the guiding-center as it travels along the magnetic field is always in the $\hat{z}$ direction.

We can rectify the problem of the purely toroidal magnetic field by adding a poloidal component to twist the field, so that the field-lines are wound helically around nested toroidal surfaces, known as (magnetic) *flux-surfaces*. Such a helical field-line is illustrated by the black curve in Figure 2.3. If the poloidal component is small, the drift will still approximately be in the $\hat{z}$ direction, but the $\hat{z}$ directed drift will then bring the particle closer to $z = 0$ when the field-line is at $z < 0$, and away from $z = 0$ when $z > 0$, resulting in the particle returning to its original minor radius.

To mathematically describe the motion along the twisted field lines, it is convenient to introduce a coordinate system aligned with the magnetic field. We thus define a new radial coordinate, a *flux-surface label* ψ which is constant on a given flux-surface and varies across them. A common choice is to use the poloidal or toroidal flux of the magnetic field inside the given magnetic surface. To then label field-lines on a flux-surface, we introduce a second label α, which is constant for a field-line and varies between them. Finally, we introduce l as the distance along the magnetic field-line. Thus, ψ specifies a flux-surface, the pair (ψ, α) specifies a field-line on a flux-surface and the three numbers (ψ, α, l) specify a point on the flux-surface[3]. These coordinates are illustrated in Figure 2.4.

[3]On irrational flux-surfaces in a confinement device (i.e. those that do not return

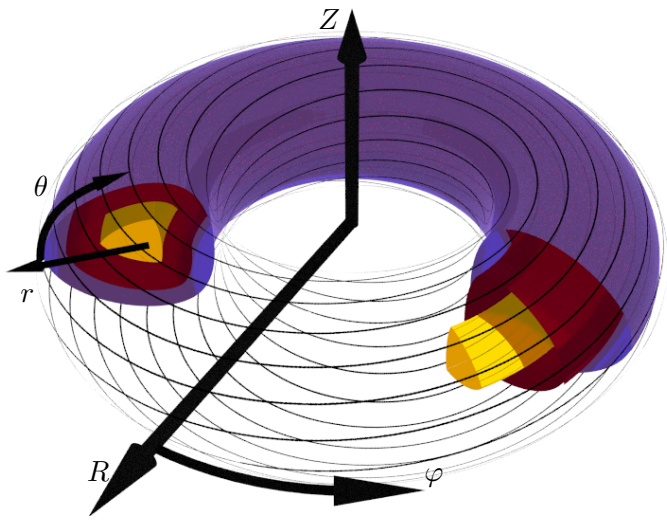

Figure 2.3: An illustration of a toroidal magnetic field with a small poloidal component, resulting in a field-line (depicted in black) being twisted around nested magnetic surfaces, which are highlighted for a section of the torus. The cylindrical coordinates $\{Z, R, \varphi\}$ and toroidal coordinates $\{\zeta = -\varphi, r, \theta\}$ are defined by arrows in the direction of increasing values of the coordinates. This is the magnetic field of a tokamak.

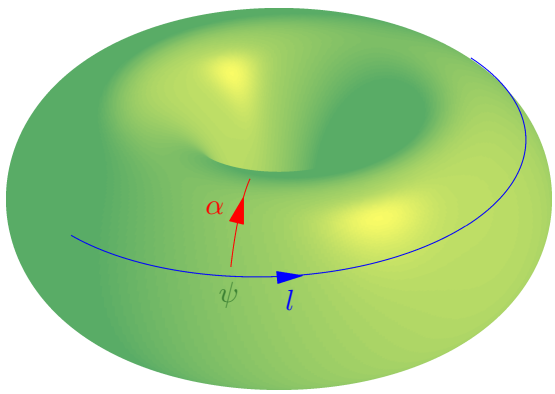

Figure 2.4: An example illustration of field-aligned coordinates (ψ, α, l), where ψ specifies the toroidal flux-surface, α specifies a given field line, and l the distance along the field-line.

To describe the effective particle motion on time-scales longer than the time it takes for a particle to complete its periodic orbit along the field-line, we average the motion of the particle over a period in l. The requirement for confining the drift orbit to the magnetic surface is to have no net drift in the ψ-direction during an orbit

$$\int \boldsymbol{v}_{\mathrm{d}} \cdot \nabla\psi \, \mathrm{d}l = 0. \tag{2.16}$$

To achieve the above condition, the magnetic field strength can no longer be constant along the field-line. Mathematically, $\nabla B \cdot \mathrm{d}\boldsymbol{l} \neq 0$, which implies a mirror force parallel to the field-line. This force will reflect particles with insufficient parallel velocity, $mv_{\parallel}^2 < \mu B_{\max}$, where $B_{\max}$ is the maximum field strength along the field-line. This leads to two classes of orbits in l: passing orbits with $mv_{\parallel}^2 > \mu B_{\max}$ complete a full-lap along the field-line, (2.16) is taken along a full-circuit. For particles with $mv_{\parallel}^2 < \mu B_{\max}$, (2.16) is taken between bounce-points. Both classes of orbits are periodic, which lets us define a *second adiabatic invariant*

$$J = \int_{l_1}^{l_2} v_{\parallel} \, \mathrm{d}l, \tag{2.17}$$

which is constant for the drift-motion over many parallel orbit periods.

This second adiabatic invariant allows us to succinctly formulate the condition in (2.16). If

$$\frac{\partial J}{\partial \alpha} = 0, \tag{2.18}$$

then orbits preserving the second adiabatic invariant will on average stay on a fixed flux-surface ψ, and the drift orbits are confined [13]. The following sections will describe various strategies for satisfying this condition.

Magnetic confinement in tokamaks

We start our discussion on confining magnetic fields by considering the tokamak, as this allows us to calculate explicit expressions for the width

to the same point after a finite number of toroidal laps), each field-line gets arbitrarily close to a given point on the flux-surface, so that a given point on the surface ψ can be specified (to any arbitrary precision) by any of an infinite number of (ψ, α, l) so that the mapping from from (ψ, α, l) to a point on the flux-surface is not invertible. This is not a problem for describing the lowest order particle dynamics in l, since both ψ and α are then constant.

of the drift-orbit; this *orbit width* is an important concept for understanding the collisional transport in any toroidal magnetic field.

In tokamaks, the condition (2.18) is satisfied by having the magnetic field be symmetric in the toroidal direction. Such a magnetic configuration is depicted in Figure 2.3, and can only be achieved by driving a current in the plasma itself.

In fact, toroidal symmetry simplifies the treatment to the extent that it becomes unnecessary to perform any orbit-averages, as we can directly deduce the radial extent of particle orbits from the Lagrangian of a single particle in a magnetic field: According to Noether's theorem, each continuous symmetry of the Lagrangian corresponds to a conserved quantity. In toroidal symmetry, this conserved quantity is the toroidal component of the canonical momentum

$$p_\zeta = Rmv_t + eRA_t = Rmv_t - Ze\psi_p. \tag{2.19}$$

Here, v_t is the toroidal component of the velocity. The poloidal flux $\psi_p = -RA_t$ is a flux-surface label, and from (2.19), we thus see that the change in ψ_p over a particle orbit, $\Delta\psi_p$, is related to the change in kinetic toroidal angular momentum over charge, $\Delta(Rmv_t/e)$. Thus, unless a particle is able to gain kinetic energy indefinitely, the particle cannot stray too far from its initial magnetic surface, and is confined. This result is known as *Tamm's theorem* [52].

This confinement is for a single particle. In a plasma, particles will interact with each other, and can thus gain or lose energy and angular momentum. Particle interactions will be the subject of Section 2.2 – naively, we can think of the particle interactions as discrete events (*collisions*) resulting in the particle taking a step $\Delta\psi_p$ to a nearby flux-surface. The rate of *collisional transport* will depend on the size of this step.

Collisional transport due to deviations $\Delta\psi_p$ from a flux-surface is known as *neoclassical transport*, to differentiate it from so-called *classical transport*, which is due to the deviations ρ between particle and guiding-center position. As neoclassical transport typically dominates over classical transport, the term is sometimes used synonymously with collisional transport in a toroidal magnetic field.

We now set out to calculate $\Delta\psi_p$. However, we first note that (2.19) involves the exact toroidal velocity of the particle – including gyration that we do not wish to resolve. The contribution from the gyration can be removed by instead considering the motion of the guiding-center.

By gyroaveraging the Lagrangian used to derive (2.19), we obtain a Lagrangian for the guiding-center motion [46], at which point Noether's theorem tells us that

$$\langle p_\zeta \rangle_{\boldsymbol{X}} = \frac{RB_t m v_\parallel}{B} - Ze\psi_p \tag{2.20}$$

is conserved for the guiding-center motion. As an order of magnitude estimate, the change in ψ_p is thus comparable to

$$\Delta\psi_p \sim \frac{mRB_t}{ZeB} v_\parallel \sim \rho RB. \tag{2.21}$$

The corresponding width in real-space can be obtained by

$$\Delta r \sim \frac{\Delta\psi}{|\nabla\psi_p|} \sim \frac{B}{B_p}\rho, \tag{2.22}$$

where we have used $\boldsymbol{B} = \nabla \times \boldsymbol{A} \implies |\nabla\psi_p| = RB_p$, with B_p being the poloidal magnetic field. We define the *poloidal gyroradius*

$$\rho_p \equiv \frac{B}{B_p}\rho, \tag{2.23}$$

which according to the above estimate sets the size of the orbit width in a tokamak.

With the above results, we are now in a position to revisit the qualitative discussion regarding global and local transport in the introduction, which will be relevant for treating the sharp gradients in the tokamak pedestal. First, we rephrase the guiding-center formalism in terms of the language of Section 1.1. Comparing (1.2) with (2.8), and identifying Δr with ρ, we see that the guiding-center formalism is *local*. However, ρ_p can be much larger than ρ if B_p/B is small, as in conventional tokamaks. It is thus possible to have situations which are local to a field-line – i.e. when ρ is small and guiding-center motion applies – but still non-local in the radial coordinate ψ due to a large $\Delta r \sim \rho_p$, compared to the length-scale of radial variations in the plasma. We will consider such a scenario in Chapter 3, where we derive an equation describing the distribution of a large-number of guiding-centers in the presence of sharp density and electrostatic potential gradients.

Magnetic confinement in stellarators

The stellarator, unlike the tokamak, does not have a strong internal current in the plasma, which means that it is impossible to achieve

the helically twisted toroidal field while having a symmetric magnetic field [12]. Even without a symmetry in the magnetic field, there are several ways to satisfy the symmetry condition of the second adiabatic invariant, (2.18), to a high degree of accuracy.

The conceptually simplest method is known as *quasi-symmetry*, where the magnetic field strength B, rather than the magnetic field $\boldsymbol{B}$, is kept symmetric with respect to the *Boozer angles* [13, 53]. Such fields can be generated analytically through the Garren-Boozer formalism [54], or numerically by minimizing the symmetry breaking components of B. A more general class of magnetic fields are *omnigenous* fields that directly minimize (2.18). It is possible to derive analytical expressions for the collisional transport in fields that are either quasisymmetric [55] or omnigenous [56].

There are more aspects that go into designing magnetic fields, both for tokamaks and stellarators: The magnetic field has a dynamics of its own, and will respond to the pressures and currents in the plasma, which can lead to instabilities [57]. In this thesis, we will assume that such magnetohydrodynamic (MHD) optimizations – in addition to the optimization for single particle confinement described in this section – have been adequately performed, so that it becomes meaningful to study the weaker effects that degrade the confinement on time-scales longer than the time it takes for the magnetic field to disrupt. This weaker degradation of confinement is the collisional transport that we briefly sketched at the end of the previous section.

To facilitate a quantitative description of particle interactions and collisions, the next section describes how interactions between the large number of particles in a plasma can be treated statistically.

2.2 Kinetic theory and collision operators

In the previous section, we considered the motion of a single charged particle in a magnetic field. In this section, we will account for interactions among the many particles of a fusion plasma.

In a plasma, particles interact with each other through long-range electromagnetic forces. The result is an electromagnetic N-body problem. For a fusion plasma, number densities are typically of the order $10^{20}\,\mathrm{m}^{-3}$, which means that N will be a very large number. This makes it practically impossible to solve for the motion of individual particles, as we have done above.

However, because N is so large, we can make use of the machinery of statistical mechanics and consider a smooth distribution function in phase-space, that captures the large-scale behavior of our system.

For a statistical treatment, it is useful to express the N-body problem in terms of a Klimontovich equation

$$\frac{\partial}{\partial t} f_{\text{exact}}(t, \boldsymbol{x}, \boldsymbol{v}) + \boldsymbol{v} \cdot \frac{\partial}{\partial x} f_{\text{exact}}(t, \boldsymbol{x}, \boldsymbol{v}) + \boldsymbol{a} \cdot \frac{\partial}{\partial v} f_{\text{exact}}(t, \boldsymbol{x}, \boldsymbol{v}) = 0, \quad (2.24)$$

where $f_{\text{exact}} = \sum_i^N \delta^3(\boldsymbol{x} - \boldsymbol{x}_i)\delta^3(\boldsymbol{v} - \boldsymbol{v}_i)$, is an exact distribution function for N point-particles, with δ the Dirac delta-function and $\boldsymbol{x}_i$ and $\boldsymbol{v}_i$ the position and velocity of particle i; $\boldsymbol{a}$ is the acceleration at phase-space coordinates $(\boldsymbol{x}, \boldsymbol{v})$ – itself a functional of f_{exact} as the particles themselves generate electromagnetic fields.

We can identify the differential operator in the Klimontovich equation as the convective derivative in phase-space $\frac{\mathrm{d}}{\mathrm{d}t} \equiv \frac{\partial}{\partial t} + \sum_{i=1}^{6} \dot{z}_i \frac{\partial}{\partial z_i}$, where $\boldsymbol{z} = \{\boldsymbol{x}, \boldsymbol{v}\}$ denotes the position in 6-dimensional phase-space. With this identification, (2.24) follows directly from Liouville's theorem [58].

The N-particle system can be equivalently expressed in terms of n-body distribution functions through the Bogoliubov–Born–Green–Kirkwood–Yvon (BBGKY) hierarchy [59]. These n-body distribution functions give the joint probability of finding n particles in infinitesimal regions around n given points in phase-space, and are thus smooth functions. The calculation of such probabilities relies on assigning probabilities to appropriate microstates, typically by assuming the ergodic hypothesis to hold. The equation for the n-body distribution function involves the $(n+1)$-body distribution function, and thus we still have N coupled differential equations, as required for this system to be equivalent to the N-particle problem.

The advantage of the BBGKY hierarchy is that, under certain conditions, it can be truncated to yield an equation for a smooth 1-particle distribution function f. The argument is similar to the multiple time-scale expansion we will perform in the following section, and can be sketched as follows:

In the scenario of interest, where collective effects dominate, the dynamics of the $(n > 1)$-body functions is much faster than that of the 1-body function. The 1-body dynamics can then be neglected for the purpose of solving for the $(n > 1)$-body functions – in particular, the 2-body function can be expressed solely in terms of the instantaneous value of the 1-body function. Thus it becomes possible to rewrite the

2-body term in the equation governing the 1-body function f in terms of the 1-body function itself, yielding a single equation for the 1-body probability distribution function known as the *kinetic equation*:

$$\frac{\partial}{\partial t} f(t, \boldsymbol{x}, \boldsymbol{v}) + \boldsymbol{v} \cdot \frac{\partial}{\partial x} f(t, \boldsymbol{x}, \boldsymbol{v}) + \boldsymbol{a} \cdot \frac{\partial}{\partial v} f(t, \boldsymbol{x}, \boldsymbol{v}) = C[f]. \tag{2.25}$$

Equation (2.25) has essentially the same form as (2.24), but with f a smooth, macroscopic 1-particle distribution function, and with an extra term $C[f]$ that is due to the statistical description of the particle interactions. All many-particle effects depending on the detailed trajectories of the particles are accounted for by a *collision operator* C acting on f.

In general, the plasma consists of more than one species of particles, and we label each species by a subscript. In this case, the collision operator also produces a coupling between species; the net effect on species a from all species is then

$$C[f_a] = \sum_b C_{ab}[f_a, f_b]. \tag{2.26}$$

As (2.25) can be written as $\mathrm{d}f_a/\mathrm{d}t = C[f_a]$, it follows that $C[f_a]$ can be interpreted as the rate of change in f_a due to particle interactions. In magnetic fusion, during normal operation – i.e. not considering runaway phenomena [60] – the particle interactions are dominated by non-relativistic, small-momentum exchange Coulomb collisions. In this case, C_{ab} is well-approximated by a Landau Fokker-Planck collision operator [61]

$$C_{ab}[f_a, f_b] = \tag{2.27}$$
$$\frac{\ln \Lambda}{8\pi m_a} \frac{Z_a^2 Z_b^2 e^4}{\epsilon_0^2} \frac{\partial}{\partial v_k} \int \frac{u^2 \delta_{kl} - u_k u_l}{u^3} \left[\frac{f_a(\boldsymbol{v})}{m_b} \frac{\partial f_b(\boldsymbol{v}')}{\partial v_l'} - \frac{f_b(\boldsymbol{v}')}{m_a} \frac{\partial f_a(\boldsymbol{v})}{\partial v_l} \right] \mathrm{d}^3 v',$$

where $\boldsymbol{u} = \boldsymbol{v} - \boldsymbol{v}'$ is the relative velocity; δ_{kl} is the Kronecker-delta; summation over repeated indices is implied; and $\ln \Lambda \approx \ln (n\lambda_D^3)$ is the Coulomb logarithm, with $\lambda_D = \sqrt{\epsilon_0 T/(ne^2)}$ the Debye length, where ϵ_0 is the permittivity of free space, T the temperature, and n the density of the plasma. With C given by (2.27), the kinetic equation (2.25) is known as the *Fokker-Planck equation*, which is fundamental to many kinetic studies in magnetic fusion.

In the scenario considered above, the condition that collective effects dominate can be conveniently expressed in terms of the number of particles in a sphere of radius λ_D. If this number is much greater than

one, a charge in the plasma is effectively screened on distances longer than λ_D, so that the plasma looks neutral on macroscopic scales. As λ_D is typically 10^{-4} m or smaller in a fusion plasma, the plasma is effectively neutral on length-scales relevant for transport phenomena, and the distribution functions thus obey the neutrality condition

$$\sum_a Z_a \int \mathrm{d}^3 v f_a = 0, \tag{2.28}$$

a relation known as *quasi-neutrality*. Here Z_a is the charge of species a given in terms of the elementary charge.

The Fokker-Planck collision operator (2.27) satisfies the conservation of particles, momentum and energy in collisions between particles a and b, which can be expressed as

$$\int \mathrm{d}^3 v C_{ab}[f_a, f_b] = 0, \tag{2.29}$$

$$\int \mathrm{d}^3 v m_a \boldsymbol{v} C_{ab}[f_a, f_b] = -\int \mathrm{d}^3 v m_b \boldsymbol{v} C_{ba}[f_b, f_a], \tag{2.30}$$

$$\int \mathrm{d}^3 v \frac{m_a v^2}{2} C_{ab}[f_a, f_b] = -\int \mathrm{d}^3 v \frac{m_b v^2}{2} C_{ba}[f_b, f_a]. \tag{2.31}$$

These relations are useful to simplify analytic calculations and to verify that simulations are conservative. In this thesis, (2.30) will be used to relate the friction force on impurities colliding with bulk hydrogen ions to the friction force on bulk hydrogen ions colliding with impurities.

Although the Fokker-Planck equation is a vast simplification over the N-body problem, the collision operator (2.27) is often too complicated to allow analytic solutions or for implementation in codes. In the limit where a species a with temperature T_a is much lighter than a species b with temperature $T_b \sim T_a$, their collision operator C_{ab} can be simplified by expanding in their mass-ratio. The resulting mass-ratio expanded collision operator

$$C_{ab} = \nu_{ab}^D(v) \left(\mathcal{L}(f_{a1}) + \frac{m_a \boldsymbol{v} \cdot \boldsymbol{V}_b}{T_a} f_{a0} \right), \tag{2.32}$$

is frequently used to simplify calculations where electrons collide with ions, or when ions collide with much heavier ions – such as hydrogen colliding with heavy impurities in fusion plasma. Here, $\nu_{ab}^D(v)$ is a velocity dependent deflection frequency

$$\nu_{ab}^D(v) = \frac{n_b Z_a^2 Z_b^2 e^4 \ln \Lambda}{4\pi m_a^2 \epsilon_0^2 v^3}, \tag{2.33}$$

where n and e are the density and charge of the species indicated by the subscript; $\mathcal{L}$ is the Lorentz differential operator [61]; and $\boldsymbol{V}_b$ is the flow velocity of species b (to be defined in Section 2.2.1).

Another frequently employed simplification of the Fokker-Planck equation is to order the collision operator large or small compared to other terms in (2.25). To quantify the size of the collision operator, it is useful to define a typical collision frequency

$$\nu_{ab} = \frac{n_b Z_a^2 Z_b^2 e^4 \ln \Lambda}{4\pi m_a^2 \epsilon_0 v_{Ta}^3}, \tag{2.34}$$

which is simply the deflection frequency $\nu_{ab}^D(v)$ for a particle at the thermal speed $v_{Ta} \equiv \sqrt{2T_a/m_a}$, where T_a is the temperature of f_a. We will discuss both the limits where $\nu_a \equiv \sum_a \nu_{ab}$ is much larger or smaller than the frequency of a drift-orbit in Section 2.3.2. In the next section, we show how the distribution function f can be used to calculate transport of particles, momentum and energy.

2.2.1 Transport moments

From the macroscopic distribution function f, we can calculate any macroscopic plasma quantity by taking velocity moments. Some of the most often used moments are,

$$\text{Density} \qquad n = \int \mathrm{d}^3 v\, f, \tag{2.35}$$

$$\text{Particle flux} \qquad \boldsymbol{\Gamma} = \int \mathrm{d}^3 v\, \boldsymbol{v} f, \tag{2.36}$$

$$\text{Momentum flux} \qquad \overleftrightarrow{\boldsymbol{\Pi}} = m \int \mathrm{d}^3 v\, \boldsymbol{v}\boldsymbol{v} f, \tag{2.37}$$

$$\text{Heat flux} \qquad \boldsymbol{Q} = \frac{m}{2} \int \mathrm{d}^3 v\, \boldsymbol{v} v^2 f. \tag{2.38}$$

From the particle flux, we also define the *flow velocity* $\boldsymbol{V} \equiv \boldsymbol{\Gamma}/n$.

Often, a distinction is made between velocity moments taken in the "lab frame" (as above), and moments taken in the frame moving with the plasma fluid-flow velocity of each species, $\boldsymbol{v} \to \boldsymbol{v} - \boldsymbol{V}$. The pressure is defined relative to the flow velocity

$$p = \frac{m}{3} \int \mathrm{d}^3 v\, (\boldsymbol{v} - \boldsymbol{V})^2 f, \tag{2.39}$$

from which we define the temperature as $T \equiv p/n$. The *conductive heat flux* is defined as

$$\boldsymbol{q} = \frac{m}{2}\int \mathrm{d}^3v\,(\boldsymbol{v}-\boldsymbol{V})|\boldsymbol{v}-\boldsymbol{V}|^2 f. \tag{2.40}$$

which can be related to the heat flux $\boldsymbol{Q}$ by

$$\boldsymbol{q} = \boldsymbol{Q} - \frac{5}{2}p\boldsymbol{V} - \frac{1}{2}nmV^2\boldsymbol{V} - (\overleftrightarrow{\boldsymbol{\Pi}}\cdot\boldsymbol{V} - p\boldsymbol{V})\,; \tag{2.41}$$

note that the $(\overleftrightarrow{\boldsymbol{\Pi}}\cdot\boldsymbol{V} - p\boldsymbol{V})$ term often is small in a confined plasma.

We will consider scenarios when the flow is small compared to the thermal speed, so the distinction between lab frame and fluid-flow frame is mostly unimportant, except for the heat flux, where the first two terms in (2.41) are comparable in size, so that $\boldsymbol{q} \approx \boldsymbol{Q} - \frac{5}{2}p\boldsymbol{V}$.

The goal of transport theory is often simply to calculate the above moments to evaluate the confinement of particles, momentum and heat. We can get equations directly relating the moments among themselves by taking moments of the kinetic equation (2.25). The first few moments obey:

$$\frac{\partial n}{\partial t} + \nabla\cdot\boldsymbol{\Gamma} = 0 \tag{2.42}$$

$$m\frac{\partial \boldsymbol{\Gamma}}{\partial t} + \nabla\cdot\overleftrightarrow{\boldsymbol{\Pi}} - e\,(n\boldsymbol{E} + \boldsymbol{\Gamma}\times\boldsymbol{B}) = \boldsymbol{F}_c \tag{2.43}$$

$$\frac{3}{2}\frac{\partial}{\partial t}\left(p + \frac{mV^2}{2}\right) + \nabla\cdot\boldsymbol{Q} = W_c + e\boldsymbol{\Gamma}\cdot\boldsymbol{E}, \tag{2.44}$$

which describe the conservation of particles, momentum and energy. Here, we have introduced the moments of the collision operator $\boldsymbol{F_c} = \int \mathrm{d}^3v\, m\boldsymbol{v}C[f]$ and $W_c = \int \mathrm{d}^3v\,\frac{m}{2}v^2 C[f]$ – the friction force density and the collisional energy exchange.

The collision operator acts as an effective source-term in (2.43) and (2.44): Since the collisions we consider do not convert particles between different species, there is no source of particles due to collisions in (2.42). Likewise, since energy and momentum are conserved in each collision (2.30)-(2.31), the sum of the friction force and collisional energy exchange over all species is zero. If the plasma is fueled with particles and energy externally – or if fusion reactions occur – we add source terms to the kinetic equation, which will contribute to the moment equations above.

The moment equations are more convenient than the kinetic equation, as they are expressed in 3-dimensional real-space – rather than 6-dimensional phase-space – and directly describe the fluxes of particles, momentum, heat, etc. However, they cannot be evaluated without a *closure*. Specifically, each moment equation in (2.42)–(2.44) couples to higher moment equations, analogously to the n-body distribution functions in the BBGKY hierarchy. Thus we need to evaluate or approximate one of the higher moments to close the set of equations.

A rigorous closure is difficult to find in general. When collisions dominate, the Chapman-Enskog method [62] can be employed, yielding the Braginskii fluid equations [63]. However, this closure is not applicable to the hundred-million degrees center of a tokamak plasma, and thus we have to face up to the kinetic equation (2.25). In the next section, we will approximate and simplify the kinetic equation in a manner appropriate for quiescent magnetized plasmas, the result of which is the *drift-kinetic equation*. The moment equations can then be used to relate the different moments of the distribution function in (2.35)-(2.40), and even to calculate moments of the distribution function to higher precision than that which is possible through the drift-kinetic equation alone.

2.3 The drift-kinetic equation

In Section 2.1, we described how the motion of a particle in magnetic fields that vary weakly over the gyroradius scale can be decomposed into gyration and guiding-center motion, where the latter was found to be approximately independent of the gyrophase. The same is also true for the distribution function, provided that the gyration is faster than all other time-scales of interest.

To connect our single-particle results to the kinetic description, we first note that the left-hand side of the kinetic equation (2.25) is invariant under coordinate transformations on phase-space $\boldsymbol{z} \to \boldsymbol{z}'$, so that we can use the *guiding-center coordinates*

$$\boldsymbol{X} = \boldsymbol{x} - \boldsymbol{\rho}, \tag{2.45}$$

$$W \equiv \frac{mv^2}{2} + Ze\Phi, \tag{2.46}$$

$$\mu = \frac{mv_\perp^2}{2B}, \tag{2.47}$$

$$\gamma = -\arctan\left(\frac{v_2}{v_1}\right), \tag{2.48}$$

where $\boldsymbol{\rho} = \frac{\boldsymbol{b}(\boldsymbol{X})\times\boldsymbol{v}}{\Omega(\boldsymbol{X})}$ is the gyro-radius vector evaluated at $\boldsymbol{X}$. W is the energy of a particle at point $\boldsymbol{x}, \boldsymbol{v}$ in velocity space, μ is the magnetic moment; γ is an azimuthal angle in velocity space. These definitions are essentially the same as in Section 2.1, except that $v_\perp$ here is the exact perpendicular velocity, unlike (2.3) and (2.5) which exclude the drifts.

Performing the change of coordinates

$$\{\boldsymbol{x}, \boldsymbol{v}\} \to \{\boldsymbol{X}, W, \mu, \gamma\}, \tag{2.49}$$

the kinetic equation (2.25) becomes

$$\dot{f}_a = \frac{\partial}{\partial t} f_a + \dot{\boldsymbol{X}} \cdot \frac{\partial}{\partial \boldsymbol{X}} f_a + \dot{W}\frac{\partial f}{\partial W} + \dot{\mu}\frac{\partial f}{\partial \mu} + \dot{\gamma}\frac{\partial f}{\partial \gamma} = C[f_a], \tag{2.50}$$

where a dot represents a time derivative along a phase-space trajectory

$$\dot{A} = \frac{\partial A}{\partial t} + \boldsymbol{v} \cdot \frac{\partial A}{\partial \boldsymbol{x}} + \boldsymbol{a} \cdot \frac{\partial A}{\partial \boldsymbol{v}}, \tag{2.51}$$

with $\boldsymbol{a}$ the acceleration at $\{\boldsymbol{x}, \boldsymbol{v}\}$.

Just as in the single particle case, the guiding-center dynamics will provide a simplification if the gyration dominates over all other time-scales of interest. When that is the case, (2.50) becomes, to lowest order,

$$\dot{\gamma}\frac{\partial f}{\partial \gamma} = 0, \tag{2.52}$$

which tells us that the distribution function is approximately independent of γ. This is a central result, although a less crude approximation to the kinetic equation is needed to find the dependence of f on the other variables.

2.3.1 Approximations and ordering assumptions

To apply a perturbation analysis to the kinetic equation, we need to introduce a formal small parameter ϵ. As in Section 2.1.1, we assume that the magnetic field varies little on the gyroradius-scale, $\epsilon \equiv \rho/L_B \ll 1$, where $L_B = |\nabla \log B|^{-1}$ is the gradient scale-length of B. We here use ρ to denote the (bulk ion) thermal gyroradius $\rho = mv_T/(eB)$, which represents a typical gyroradius in the plasma[4]. In this section, we will order

[4]This assumes a low flow velocity, so that v_T is representative of a typical particle velocity. The same expansion parameter can also be used in plasma with sonic flows, but the transformation to a frame rotating with the flow velocity introduces some additional terms, see Ref. [64, 65].

Table 2.1: Orderings assumed when deriving the drift-kinetic equation. Definitions of the various quantities are standard and introduced throughout the thesis.

Length-scale of $\boldsymbol{B}$	$L_B \equiv \lvert\nabla \log B\rvert^{-1}$
Expansion parameter	$\epsilon \equiv \rho/L_B \ll 1$
Parallel gradients	$v_\parallel \boldsymbol{b}\cdot\nabla = \mathcal{O}(\epsilon\Omega)$
Perpendicular gradients	$\boldsymbol{v}_\perp\cdot\nabla = \mathcal{O}(\epsilon\Omega)$
Collision operator	$C[f] \sim \nu f = \mathcal{O}(\epsilon\Omega f)$
Parallel electric field	$\frac{e}{m}E_\parallel = \mathcal{O}(\epsilon\Omega v_T)$
Perpendicular electric field	$\frac{e}{m}E_\perp = \mathcal{O}(\epsilon\Omega v_T)$
Time derivatives	$\frac{\partial}{\partial t} = \mathcal{O}\left(\epsilon^3\Omega\right)$

the other quantities in (2.50) in terms of this ϵ. We quantify the statement that gyration dominates other time-scales by ordering the transit frequency $\omega_t \equiv v_T/L_B \sim \epsilon\Omega$, which is the characteristic frequency at which a thermal particle travels a distance on which B may have order unity variations (typically the size of the magnetic confinement device). We also order the effects of collisions, quantified by a collision frequency ν, as $\nu \sim \epsilon\Omega$, and assume that the Lorentz force due to the electric field is weaker than that of the magnetic field $\boldsymbol{E} \sim \epsilon v_T B \sim \epsilon\frac{m}{e}\Omega v_T$. These requirements essentially state that the magnetic field dominates the particle dynamics, which is practically a requirement for magnetic confinement. We will also assume steady-state, in the sense that $\frac{\partial}{\partial t} = \mathcal{O}\left(\epsilon^3\Omega\right)$, so that we can neglect all time-derivatives. We summarize these assumptions in Table 2.1. For a more detailed derivation, see, for example, Ref. [42].

To relate these orderings to (2.50), we rewrite the velocity-space time-derivatives in terms of the electromagnetic fields [42]

$$\dot{\mu} = -\mu\overbrace{\frac{1}{B}\boldsymbol{v}\cdot\nabla B}^{\epsilon\Omega} - \frac{v_\parallel}{B}\boldsymbol{v}_\perp\cdot\overbrace{(\boldsymbol{v}\cdot\nabla)\boldsymbol{b}}^{\epsilon\Omega} + \overbrace{\frac{Ze}{mB}\boldsymbol{v}_\perp\cdot\boldsymbol{E}}^{\epsilon\Omega\mu} \tag{2.53}$$

$$\dot{W} = \frac{Ze}{m}\boldsymbol{v}\cdot\nabla\Phi + \frac{Ze}{m}\boldsymbol{v}\cdot\boldsymbol{E} = \frac{Ze}{m}\boldsymbol{v}\cdot\overbrace{\frac{\partial\boldsymbol{A}}{\partial t}}^{\epsilon^3\Omega\boldsymbol{A}} \tag{2.54}$$

$$\dot{\gamma} = \Omega + \frac{v_\parallel}{v_\perp}\hat{\rho}\cdot\overbrace{(\boldsymbol{v}\cdot\nabla)\boldsymbol{b}}^{\epsilon\Omega} + \boldsymbol{e}_3\cdot\overbrace{\dot{\boldsymbol{e}}_2}^{\epsilon\Omega} - \overbrace{\frac{Ze}{mv_\perp}\hat{\rho}\cdot\boldsymbol{E}}^{\epsilon\Omega}, \tag{2.55}$$

where $\hat{v}_\perp = \boldsymbol{v}_\perp / v_\perp$ and $\hat{\rho} = \boldsymbol{\rho}/\rho$ and the order of the different terms are indicated with an overbrace.

As shown in Chapter 2, the velocity of the guiding-center is given by

$$\dot{\boldsymbol{X}} = \overbrace{v_\parallel \boldsymbol{b}}^{\epsilon \Omega L_B} + \overbrace{\frac{\boldsymbol{E} \times \boldsymbol{B}}{B^2}}^{\epsilon^2 \Omega L_B} + \overbrace{\boldsymbol{v}_\mathrm{m}}^{\epsilon^2 \Omega L_B}, \tag{2.56}$$

where the third term, $\boldsymbol{v}_m$, is the magnetic drift due to the mirror and centrifugal forces.

2.3.2 Hazeltine's recursive drift-kinetic equation

From the orderings of the previous section, one can derive the drift-kinetic equation (DKE). Following Hazeltine's recursive derivation [42, 66] the DKE takes the form

$$(\boldsymbol{v}_\parallel + \boldsymbol{v}_d + \boldsymbol{u}_d) \cdot \nabla \bar{f} + \left.\frac{\mathrm{d}\mu}{\mathrm{d}t}\right|_{gc} \frac{\partial \bar{f}}{\partial \mu} = C[\bar{f}], \tag{2.57}$$

where $\boldsymbol{v}_\mathrm{d}$ is the perpendicular drift-velocity (2.12), $\boldsymbol{u}_d$ is a parallel drift,

$$\left.\frac{\mathrm{d}\mu}{\mathrm{d}t}\right|_{gc} = \frac{v_\parallel \mu B}{\Omega} \boldsymbol{b} \cdot \nabla \left(\frac{v_\parallel \boldsymbol{b} \cdot \nabla \times \boldsymbol{b}}{B} \right), \tag{2.58}$$

is the change in magnetic moment as seen by the guiding-center; $\bar{f}$ is the gyroaveraged distribution keeping the exact particle position fixed, rather than the guiding-center. In (2.57), partial derivatives are taken with $\boldsymbol{x}$, W, μ and γ as coordinates.

From $\bar{f}$, the gyrophase-dependent distribution function can be obtained from [42]

$$\begin{aligned} f = \bar{f} - \boldsymbol{\rho} \cdot \left[\nabla \bar{f} + Ze\boldsymbol{b} \times \boldsymbol{v}_\mathrm{d} \frac{\partial \bar{f}}{\partial \mu} \right] \\ + \frac{v_\parallel \mu}{\Omega} \frac{\partial \bar{f}}{\partial \mu} \left[\hat{\rho} \hat{v}_\perp : \nabla \boldsymbol{b} - \frac{1}{2} \boldsymbol{b} \cdot \nabla \times \boldsymbol{b} \right] + \mathcal{O}\left(\epsilon^2 \bar{f}\right), \end{aligned} \tag{2.59}$$

where $\hat{\rho}$ and $\hat{v}_\perp$ are the unit vectors in the gyroradius direction and in the $\boldsymbol{v}_\perp$ direction. Solving (2.57) for $\bar{f}$ thus gives the gyrophase-dependent distribution function to order $\epsilon \bar{f}$ through (2.59).

Equation (2.57) is not derived through a perturbation series, and thus contains terms of different order in ϵ; it is accurate to order ϵ but captures some additional $\mathcal{O}\left(\epsilon^2 f\right)$ terms [67]. The presence of these higher

order terms makes (2.57) a convenient starting point for constructing a radially-global, linearized DKE suitable for describing the sharp gradient regions in a tokamak, which is the subject of the next chapter. For other purposes, the higher order terms can be neglected, which yields the more commonly used DKE

$$(\boldsymbol{v}_{\|} + \boldsymbol{v}_d) \cdot \nabla \bar{f} = C[\bar{f}]. \tag{2.60}$$

Solving this equation order-by-order in ϵ, the lowest order equation states that

$$\boldsymbol{v}_{\|} \cdot \nabla \bar{f}_0 = C[\bar{f}_0], \tag{2.61}$$

which implies that the zeroth-order distribution is a Maxwell-Boltzmann distribution constant on the flux-surface

$$\begin{aligned} f_M(\psi, W) &= \eta(\psi) \left(\frac{m}{2\pi T(\psi)} \right)^{3/2} \mathrm{e}^{-\frac{W}{T}} \\ &= n \left(\frac{m}{2\pi T(\psi)} \right)^{3/2} \mathrm{e}^{-\frac{mv^2}{2T}}, \end{aligned} \tag{2.62}$$

where n is the density of the Maxwellian, T the temperature, and $\eta(\psi) = n\mathrm{e}^{Ze\Phi/T}$ is the *pseudo-density*, that is more convenient when Φ varies on the flux-surface, or for evaluating derivatives with W held fixed. The above Maxwell-Boltzmann distribution is not completely general, as it does not contain any flow-velocity, which is consistent with the low-flow ordering we adopted in our derivation of the DKE, where we assumed that the flows are small compared to the thermal speed, $|\boldsymbol{V}| \sim \epsilon v_{\mathrm{T}}$.

To next order in ϵ, we find that

$$\boldsymbol{v}_{\|} \cdot \nabla \bar{f}_1 + \boldsymbol{v}_{\mathrm{d}} \cdot \nabla \bar{f}_0 = C[\bar{f}_1], \tag{2.63}$$

which is the equation that will be used to derive the transport of a highly-charged impurity species in a stellarator in Chapter 4.

Collisionality regimes

Even after expanding the drift-kinetic equation in ϵ, the resulting equation (2.63) is generally too difficult to solve analytically. To make progress, an additional expansion is typically performed in *collisionality*, which measures the relative size of the right-hand and left-hand sides of (2.63). Specifically, the collisionality $\hat{\nu}$ is defined as the ratio

of the collision frequency and the frequency at which a thermal particle completes an orbit along the field line

$$\hat{\nu}_a = \frac{\nu_a}{v_{\mathrm{T}}/L_\parallel}, \tag{2.64}$$

where $L_\parallel$ is an effective length-scale for variations in the plasma along the magnetic field-line. The collision frequency, ν_a, is the sum of the collision frequencies with all species $\nu_a = \sum_b \nu_{ab}$, where ν_{ab} is the a-b collision frequency (2.34).

High-collisionality regime For $\hat{\nu} \gg 1$, we are in the *high-collisionality* or Pfirsch-Schlüter regime, where collisions dominate the single-particle dynamics. In this regime, we expand the distribution function in $1/\hat{\nu}$ [68],

$$\bar{f}_1 = \bar{f}_1^{(-1)} + \bar{f}_1^{(0)} + \mathcal{O}\left(\bar{f}_1^{(0)}/\hat{\nu}\right) \tag{2.65}$$

where the $(1/\hat{\nu}_a)^{-2}$-order equation gives $C[\bar{f}_1^{(-1)}] = 0$ so that $\bar{f}_1^{(-1)}$ is in a local thermodynamic equilibrium, meaning that it has a Maxwellian distribution, which unlike $\bar{f}_0$, is not necessarily constant on the flux-surface. To determine how $\bar{f}_1^{(-1)}$ varies on the flux-surface, the $(1/\hat{\nu})^{-1}$ and $(1/\hat{\nu})^0$ order equations are needed: The lowest order $\bar{f}_1$ is not fully specified by the lower order equation, but as they enter as source-terms to the higher-order equations, they are constrained by the requirements that these equations should have solutions. Such requirements are known as a *solvability conditions* – see for example Ref. [69].

Low-collisionality regime For $\hat{\nu}_a \ll 1$, we are in a *low-collisionality* regime. Here, the distribution function is expanded in $\hat{\nu}$ as

$$\bar{f}_1 = \bar{f}_1^{(-1)} + \bar{f}_1^{(0)} + \mathcal{O}\left(\bar{f}_1^{(0)}\hat{\nu}\right), \tag{2.66}$$

where a $\mathcal{O}\left(\hat{\nu}^{-1}\bar{f}_1^{(0)}\right)$ term is needed to describe magnetic configurations that are not omnigenous. At $\mathcal{O}\left(\hat{\nu}^{-1}\right)$, the collision operator can be neglected, and we have

$$v_\parallel \nabla_\parallel \bar{f}_1^{(-1)} = 0, \tag{2.67}$$

which merely states that $\bar{f}_1^{(-1)}$ is constant along field-lines. The $\mathcal{O}\left(\hat{\nu}^0\right)$ equation is

$$v_\parallel \nabla_\parallel \bar{f}_1^{(0)} + \boldsymbol{v}_d \cdot \nabla \bar{f}_0 = C[\bar{f}_1^{(-1)}], \tag{2.68}$$

where the drift term $\boldsymbol{v}_d \cdot \nabla \bar{f}_0$ explains why $\bar{f}_1^{(-1)}$ is needed: For magnetic-field configurations that are not omnigenous, the orbit-average of $\boldsymbol{v}_d \cdot \nabla \bar{f}_0$ does not vanish for trapped particles, and the collision operator term containing $\bar{f}_1^{(-1)}$ is needed to balance this term. From the $\mathcal{O}\left(\hat{\nu}^1\right)$ equation,

$$v_\parallel \nabla_\parallel \bar{f}_1^{(1)} = C[\bar{f}_1^{(0)}], \tag{2.69}$$

we obtain the solvability condition for $\bar{f}_1^{(0)}$.

2.3.3 Transport moments revisited

In Section 2.2.1, we introduced fluxes and other fluid quantities, in terms of moments of f, and derived equations directly describing the evolution of these moments. We now rephrase these results in terms of the gyroaveraged distribution function $\bar{f}$ obtained from the drift-kinetic equation (2.60) – adapted to the magnetic geometry of toroidal confinement systems – to calculate the particle, momentum, and heat fluxes in the confinement system.

Inserting (2.59), the relation between $\bar{f}$ and f, into the expressions for the fluxes (2.36)-(2.38) yields the neoclassical particle, toroidal angular momentum, and heat fluxes

$$\text{Particle flux} \qquad \boldsymbol{\Gamma} = \int \mathrm{d}^3 v \, \boldsymbol{v}_d \bar{f}, \tag{2.70}$$

$$\text{Toroidal angular momentum flux} \qquad \boldsymbol{\Pi}_\zeta = m \int \mathrm{d}^3 v \, \boldsymbol{v}_d R\hat{\zeta} \cdot \boldsymbol{v}_\parallel \bar{f}, \tag{2.71}$$

$$\text{Heat flux} \qquad \boldsymbol{Q} = \frac{m}{2} \int \mathrm{d}^3 v \, \boldsymbol{v}_d v^2 \bar{f}, \tag{2.72}$$

where $\hat{\zeta}$ is the unit-vector in the toroidal direction and $\boldsymbol{\Pi}_\zeta = R\hat{\zeta} \cdot \overleftrightarrow{\boldsymbol{\Pi}}$ with R the major radius. Note that these differ from the total fluxes as they lack the magnetization fluxes [42] – which are not important for transport purposes as they are divergence free – and the classical transport, which requires a higher order version of (2.59) [70], but is more easily calculated in a fluid picture as we will show in Chapter 4.

To calculate the total flux escaping from the plasma volume bounded by the flux-surface labeled by ψ, we project the fluxes onto $\nabla\psi$ and integrate over the flux-surface. For the latter purpose, it is convenient to define a *flux-surface average*. This integral needs to be defined with some care, as a surface is a null-set and thus contains zero particles. Thus, we define the *flux-surface average* as the average over the volume

$\mathrm{d}V$ between two infinitesimally separated flux-surfaces labeled by ψ and $\psi + \mathrm{d}\psi$, which we express mathematically as

$$\langle A \rangle = \frac{1}{dV} \int_{dV} A \, \mathcal{J} \mathrm{d}\psi \mathrm{d}\theta \mathrm{d}\psi = \frac{1}{V'} \oint \oint A \, \mathcal{J} \mathrm{d}\theta \mathrm{d}\zeta \tag{2.73}$$

where $V' = \mathrm{d}V/\mathrm{d}\psi$ and $\mathcal{J}$ is the Jacobian of the $\{\zeta, \psi, \theta\}$ coordinates. For a tokamak, the Jacobian is $\mathcal{J} = 1/|\boldsymbol{B}_\mathrm{p} \cdot \nabla\theta|$. The flux-surface average satisfies the following properties

$$\langle \nabla \cdot \boldsymbol{A} \rangle = \frac{1}{V'} \frac{\mathrm{d}}{\mathrm{d}\psi} \left(V' \langle \boldsymbol{A} \cdot \nabla\psi \rangle \right), \tag{2.74}$$

$$\langle \boldsymbol{B} \cdot \nabla X \rangle = 0, \tag{2.75}$$

$$\langle (\boldsymbol{B} \times \nabla) \cdot \nabla X \rangle = 0, \tag{2.76}$$

where the last two properties hold for any single-valued X, and (2.76) relies on there being no radial current – a consequence of the momentum equation (2.43) with the lowest order distribution (2.62), summed over all species – so that $\nabla \times \boldsymbol{B} \cdot \nabla\psi = 0$.

In terms of the flux-surface average, the total radial fluxes of particle, energy, and toroidal angular momentum through a flux-surface thus become

$$V' \langle \boldsymbol{\Gamma} \cdot \nabla\psi \rangle = V' \left\langle \int \mathrm{d}^3 v \, \boldsymbol{v}_d \cdot \nabla\psi \bar{f} \right\rangle \tag{2.77}$$

$$V' \langle \boldsymbol{Q} \cdot \nabla\psi \rangle = V' \left\langle \int \mathrm{d}^3 v \, \boldsymbol{v}_d \cdot \nabla\psi \frac{mv^2}{2} \bar{f} \right\rangle \tag{2.78}$$

$$V' \langle R\hat{\zeta} \cdot \vec{\boldsymbol{\Pi}} \cdot \nabla\psi \rangle = V' \left\langle \int \mathrm{d}^3 v \, \boldsymbol{v}_d \cdot \nabla\psi R\hat{\zeta} \cdot \boldsymbol{v}_\parallel \bar{f} \right\rangle. \tag{2.79}$$

Chapter 3

Transport in tokamak pedestals

The drift-kinetic equation derived in the previous chapter is one of the most fundamental equations used to study collisional transport in magnetized plasmas. In this chapter, we consider a limit that can be used to derive a linearized drift-kinetic equation that captures some of the physics of the sharp-gradient regions in tokamaks, such as the pedestal.

3.1 Linear drift-kinetic equation for tokamak pedestals

We seek to adapt Hazeltine's recursive DKE (2.57) to the sharp gradient regions of the tokamak pedestal, while still linearizing the distribution function around a flux-surface Maxwell-Boltzmann distribution f_M, as in the local drift-kinetic equation, (2.63). The insistence on a linear equation is motivated by computational convenience: In general, for sharp gradients, the problem will be nonlinear – although there are exceptions to this, when the collisionality is low [71]. We will find that for a particular ordering of the pseudo-density and temperature gradients, the distribution function nevertheless stays close to f_M, and a linear description is feasible.

To achieve this, we follow Ref. [72] and exploit a separation of scales between the orbit width and the gyroradius, which was already hinted at in Section 2.1.2. Such a distinction is not always done, as the orbit

width ρ_p is proportional to the gyroradius ρ

$$\rho_p = \frac{B}{B_p}\rho, \tag{3.1}$$

but by assuming that $B_p/B \ll 1$, we can consider the situation where the distribution function f does not vary strongly on the ρ-scale – as was required in the derivation of the DKE – but where f_1 does vary appreciably on the ρ_p scale.

To proceed, we introduce a new small expansion parameter

$$\delta \equiv \frac{\rho_p}{L_B}, \tag{3.2}$$

where $\rho_p = mv_T/(ZeB_p)$ here denotes the thermal orbit width, up to some geometric factors. This expansion parameter represents the smallness of the orbit width compared to variations in the magnetic field, which we still assume to hold.

We seek a solution to (2.57) of the form

$$\bar{f} = f_0 + f_1 + \mathcal{O}\left(\delta^2 f_0\right), \tag{3.3}$$

where the subscript here refers to the order in δ: $f_1/f_0 \sim \delta$. To facilitate such a perturbative treatment, we need to order the different terms in the drift-kinetic equation (2.57) with respect to δ.

As our expansion parameter obeys $\delta = \epsilon B/B_p$, the terms of a given ϵ order in (2.57) will generally have the same order in δ. However, we will allow the electrostatic potential and f_1 to vary on the orbit-width scale ρ_p in the ψ-direction[1]

$$|\nabla\psi|\frac{\partial\Phi}{\partial\psi} \sim \frac{\Phi}{\rho_p} \sim \frac{\Phi}{\delta L_B}, \tag{3.4}$$

$$|\nabla\psi|\frac{\partial f_1}{\partial\psi} \sim \frac{f_1}{\rho_p} \sim \frac{f_1}{\delta L_B} \sim \frac{f_0}{L_B}. \tag{3.5}$$

As a result, these terms will contribute to lower order in δ than in ϵ, which is why it is convenient to start from an equation of mixed order in ϵ.

[1] The fact that f_1 is allowed to have sharp variations in (3.5), but not f_0 will be shown to be related to the validity of the linearization in (3.3): The gradient of f_0 will act as a source for f_1, and thus set the size of f_1. An f_0 varying on the ρ_p scale would cause f_1 to violate $f_1 \sim \delta f_0$ and is thus not allowed.

The different terms in (2.57) are thus ordered:

$$\boldsymbol{v}_{\mathrm{m}} \sim \boldsymbol{u}_{\mathrm{d}} \sim \delta v_T, \tag{3.6}$$

$$\left.\frac{\mathrm{d}\mu}{\mathrm{d}t}\right|_{gc} \sim \delta \mu v_T / L_B, \tag{3.7}$$

while the $\boldsymbol{E} \times \boldsymbol{B}$-drift in the θ-direction is an order lower in δ than in ϵ

$$\hat{\theta} \cdot \boldsymbol{v}_{\mathrm{E0}} \sim \hat{\theta} \cdot \boldsymbol{v}_{\|}. \tag{3.8}$$

Inserting this into (2.57) we have, to order $\mathcal{O}\left(\delta v_T f / L_B\right)$,

$$\left(\boldsymbol{v}_{\|} + \boldsymbol{v}_{\mathrm{E}}\right) \cdot \nabla\theta \frac{\partial f_0}{\partial \theta} = C[f_0]. \tag{3.9}$$

We can solve this by making the ansatz that f_0 is a stationary, flux-surface Maxwell-Boltzmann distribution, as in (2.62).

The zeroth-order distribution function is thus a flux-function (i.e. constant on a flux-surface) in the sense that ∇f_M is in the $\nabla\psi$ direction. However, these derivatives are taken with W fixed. If Φ varies on a flux-surface, the density n – which is more experimentally accessible than f_M – will also vary. Such variations have been observed experimentally [73], but are here assumed to be higher order in δ for the sake of simplicity.

Thus, we also expand the potential, and assume it to be a flux-function to zeroth-order

$$\Phi = \Phi_0(\psi) + \Phi_1(\psi, \theta) + \mathcal{O}\left(\delta^2 \Phi_0\right), \tag{3.10}$$

where $\Phi_1 \sim \delta\Phi_0$. To be specific, we will take Φ_0 as the flux-surface average of Φ. Furthermore, we assume that $\partial\Phi_1/\partial\psi \sim \delta \mathrm{d}\Phi_0/\mathrm{d}\psi$, so that Φ_1 does not vary on smaller than ρ_p scales. This is consistent with Φ_1 being set by f_1, a result which we prove at the end of this section.

With these definitions, we can eliminate Φ_1 by a change of variables $W \to W_0 = mv^2/2 + Ze\Phi_0 = W - Ze\Phi_1 + \mathcal{O}\left(\delta^2\right)$, which implies

$$\nabla f = \nabla|_{W_0} f - \frac{\partial f}{\partial W_0} Ze \, \nabla|_{W_0} \Phi_1, \tag{3.11}$$

where ∇ refers to gradients taken with W fixed, as above, and $\nabla|_{W_0}$ refers to gradients with W_0 fixed.

In (3.9), contributions from the second term on the right-hand side of (3.11) are formally small:

$$-\frac{\partial f_M}{\partial W_0} Ze \, \nabla|_{W_0} \Phi_1 \sim \frac{Ze\Phi_1}{T} \frac{f_M}{L_B} \sim \delta \frac{f_M}{L_B}, \tag{3.12}$$

where we have assumed $\nabla_\parallel \Phi_1 \sim \Phi_1/L_B$ and used $Ze\Phi_1/T \sim \delta$, which is a consequence of quasi-neutrality within flux-surfaces. Thus, we can replace W with W_0 in (2.62). Under these assumptions, f_M and n are flux-functions.

To the next order, we have

$$\begin{aligned}&(\boldsymbol{v}_\parallel + \boldsymbol{v}_{\mathrm{E0}}) \cdot \nabla\theta \left.\frac{\partial f_1}{\partial \theta}\right|_{W_0} + \boldsymbol{v}_{\mathrm{m}} \cdot \nabla\psi \left.\frac{\partial f_1}{\partial \psi}\right|_{W_0} - C_l[f_1] \\ &= -(\boldsymbol{v}_\parallel + \boldsymbol{v}_{\mathrm{E0}} + \boldsymbol{v}_m) \cdot \left(\nabla|_{W_0} f_M - \frac{Ze f_M}{T} \nabla|_{W_0} \Phi_1 \right) + \mathcal{O}\left(\delta^2\right),\end{aligned} \tag{3.13}$$

where $\boldsymbol{v}_{E0} = B^{-1}\boldsymbol{b} \times \nabla\Phi_0$ is the $\boldsymbol{E} \times \boldsymbol{B}$-velocity due to Φ_0; we have retained the drift-terms on the left-hand side due to the sharp ψ-derivatives in f_1 and Φ_0; linearized the collision operator $C[f_1] = C_l[f_1] + \mathcal{O}\left(\delta^2\right)$; and performed the change of coordinates to W_0, where the corrections to the f_1 derivatives are formally small.

We can eliminate the last Φ_1 term in (3.13) by defining the non-adiabatic response g as

$$g = f_1 + \frac{Ze\Phi_1}{T} f_M. \tag{3.14}$$

To obtain a linear description, we will assume that f_M and T vary on the L_B scale. Since f_M and T are also flux-functions, we have that

$$(\boldsymbol{v}_\parallel + \boldsymbol{v}_{\mathrm{d0}}) \cdot \nabla|_{W_0} \left(\frac{e\Phi_1}{T} f_M \right) = \frac{Ze f_M}{T} (\boldsymbol{v}_\parallel + \boldsymbol{v}_{\mathrm{d0}}) \cdot \nabla|_{W_0} \Phi_1 + \mathcal{O}\left(\delta^2\right), \tag{3.15}$$

where $\boldsymbol{v}_{\mathrm{d0}} = \boldsymbol{v}_{\mathrm{E0}} + \boldsymbol{v}_m$ is the drift velocity excluding the small contribution from Φ_1. Using (3.15) and $C_l[f_M] = 0$, the equation for g becomes

$$(\boldsymbol{v}_\parallel + \boldsymbol{v}_{\mathrm{d0}}) \cdot \nabla|_{W_0} g - C[g] = -\boldsymbol{v}_{\mathrm{m}} \cdot \nabla\psi \left.\frac{\partial f_M}{\partial \psi}\right|_{W_0} + S. \tag{3.16}$$

This is the radially-global, linearized drift-kinetic equation solved in this work. In (3.16), we have allowed for a source term S to this order; in general, radially-global transport is inconsistent with steady-state assumptions unless sources are included, as we will see in the next section. As the source was added at this order, it does not affect the derivation of (3.16).

A corresponding radially-local equation – appropriate for describing core transport – can be obtained from (3.16) if we soften the assumptions

on the radial variation in Φ and g, so that they vary on the L_B rather than the ρ_p scale. The drift term then becomes higher order in δ, and (3.16) reduces to the standard drift-kinetic equation [61]

$$\boldsymbol{v}_{\parallel} \cdot \nabla|_{W_0} g - C[g] = -\boldsymbol{v}_{\mathrm{m}} \cdot \nabla\psi \left.\frac{\partial f_M}{\partial \psi}\right|_{W_0} + S. \tag{3.17}$$

In this equation, there is no $\partial g/\partial\psi$ term: For the purpose of calculating g, ψ merely enters as a parameter, and the equation is thus radially-local; unlike in (3.16), the source term in (3.17) is not needed for consistency.

Another possibility is to retain the strong variations in Φ, but assume that g varies weakly, so that the radial $\boldsymbol{v}_m \cdot \nabla g$ term becomes formally small. This intermediate step between (3.16) and (3.17) has been studied analytically [74–77] and numerically [72]. However, the presence of strong Φ variations naturally causes g to develop strong variations unless the profiles are specifically choosen to avoid this [72]. The analytic theory can nevertheless serve as a useful benchmark for global codes, where terms can be switched off artificially.

The methods used for the numerical solution of (3.16) and (3.17) are briefly described in Section 3.3. In the remainder of this section, we will consider two aspects of the above derivation in more detail. To simplify notation, we drop the W_0 subscript on derivatives: All derivatives will be taken with W_0 fixed for the remainder of this chapter.

First, we show that $g \sim \delta f_M$. From estimating the size of the terms in (3.16), we have

$$v_T \frac{B_p}{B}\frac{g}{L_B} \sim \frac{v_T^2}{L_B \Omega}\frac{f_M}{L_M} \implies g \sim \frac{\rho_p}{L_M} f_M, \tag{3.18}$$

where L_M is the length-scale of the Maxwellian. If $L_M \sim L_B$, we thus have $g \sim \delta f_M$. As

$$\nabla\psi \left.\frac{\partial f_M}{\partial \psi}\right|_{W_0} = \nabla\psi \left[\frac{\partial \ln \eta}{\partial \psi} + \left(\frac{m W_0}{T} - \frac{3}{2}\right)\frac{\partial \ln T}{\partial \psi}\right] f_M, \tag{3.19}$$

the $L_M \sim L_B$ assumption implies that the η and T length-scales must be comparable to L_B, but strong n and Φ gradients are possible.

Note that the n (or η), T and Φ_0 profiles are effectively inputs to the equation for g. If they are chosen appropriately, then Φ_1 can be shown to be $e\Phi_1/T \sim \delta$. Specifically, by requiring that the zeroth order densities are quasi-neutral, we can estimate the size of Φ_1 by applying

quasi-neutrality to f_1

$$\sum_a \int \mathrm{d}^3 v \left(g_a - \frac{Z_a e \Phi_1}{T_a} f_{Ma} \right) = 0, \tag{3.20}$$

so that

$$\Phi_1 = \frac{1}{\sum_a \frac{Z_a e n_a}{T_a}} \sum_a \int \mathrm{d}^3 v \, g_a \implies \frac{e\Phi_1}{T} \sim \frac{g}{f_M} \sim \delta, \tag{3.21}$$

as we assumed in our derivation.

3.2 Moment equations for the pedestal

From the previous section, we have

$$\bar{f} = f_M + f_1 = f_M + g - \frac{Ze\Phi_1}{T} f_M, \tag{3.22}$$

whereupon (2.59) gives the gyrophase-dependent f in terms of f_M and g,

$$\begin{aligned} f =& f_M + g - \frac{Ze\Phi_1}{T} f_M - \boldsymbol{\rho} \cdot \nabla (f_M + g) \\ & - \boldsymbol{\rho} \cdot \left[Ze\boldsymbol{b} \times \boldsymbol{v}_{\mathrm{d}0} \frac{\partial g}{\partial \mu} \right] + \mathcal{O}\left(\delta^2 f_M\right). \end{aligned} \tag{3.23}$$

Here, we have used that $\partial f_M / \partial \mu = 0$ and ordered $\boldsymbol{\rho} \cdot \nabla (f_M + g) \sim v_\parallel |\nabla b| / \Omega \sim \delta$, as is appropriate for the global theory.

Note that the $Ze\boldsymbol{\rho} \cdot \boldsymbol{b} \times \boldsymbol{v}_{\mathrm{m}} \partial g / \partial \mu$ term in (3.23) is formally $\mathcal{O}\left(\delta^3 f_M\right)$, but needs to be retained in the divergence-flux terms ($\nabla \cdot \boldsymbol{\Gamma}$, etc.) in the moment equations (2.42)-(2.44) as it can have strong radial variations through g. This is a general issue in the global theory, where formally small terms may have large radial variations, and thus may need to be retained for the purpose of calculating gradients.

For this reason, it is useful to consider the global fluxes via moment equations derived from the drift-kinetic equation (3.16), as these equations contain the derivatives of g and thus do not neglect any required small terms. These equations will be used to verify that (3.23) contains all the required small terms.

Taking the density $\left(\int \mathrm{d}^3 v\right)$ moment of (3.16), we find [78]

$$\nabla \cdot \left(\int \mathrm{d}^3 v \, [\boldsymbol{v}_\parallel + \boldsymbol{v}_{\mathrm{d}0}] \bar{f} \right) = \int \mathrm{d}^3 v \, S, \tag{3.24}$$

where the formally small $\boldsymbol{v}_{\mathrm{m}}$ term is included as the only radial component in $\boldsymbol{v}_{\mathrm{d0}}$. If we identify the divergence term in (3.24) as $\nabla \cdot \Gamma$, this equation merely restates particle conservation (2.42) for steady state, $\partial n/\partial t = 0$, in terms of the motion of guiding-centers. Similarly, we have the energy and toroidal angular momentum conservation equations

$$\nabla \cdot \left(\int \mathrm{d}^3 v \, [\boldsymbol{v}_{\parallel} + \boldsymbol{v}_{\mathrm{d0}}] \frac{m v^2}{2} \bar{f} \right) + \left(\int \mathrm{d}^3 v \, [\boldsymbol{v}_{\parallel} + \boldsymbol{v}_{\mathrm{d0}}] \bar{f} \right) \cdot Ze \nabla \Phi_0 = \int \mathrm{d}^3 v \, \frac{m v^2}{2} S, \tag{3.25}$$

$$\nabla \cdot \left(\int \mathrm{d}^3 v \, [\boldsymbol{v}_{\parallel} + \boldsymbol{v}_{\mathrm{d0}}] \frac{I m v_{\parallel}}{B} \bar{f} \right) - Ze \int \mathrm{d}^3 v \, \bar{f} \boldsymbol{v}_{\mathrm{d0}} \cdot \nabla \psi = \int \mathrm{d}^3 v \, \frac{I m v_{\parallel}}{B} S. \tag{3.26}$$

Transport of toroidal angular momentum is of particular importance, as the total kinetic toroidal angular momentum (i.e. summed over all species) is conserved in axisymmetry, so that the plasma can only spin up or down by transporting angular momentum, or in the presence of momentum sources. As plasma rotation is important for the transition into H-mode [79], momentum transport can have important implications for the confinement properties of a reactor.

The divergence terms in (3.24)-(3.26) practically define the particle, heat and momentum fluxes. As these fluxes contain $\boldsymbol{v}_m$, we are obliged to retain this term in (3.23) to properly conserve particles, toroidal angular momentum and energy. These indirect definitions do however not capture divergence-free contributions to the fluxes. To capture those terms, we turn to the basic definition of the fluxes, i.e. (2.37). Using (3.23), the particle flux becomes [42]

$$\boldsymbol{\Gamma} = \int \mathrm{d}^3 v \, \boldsymbol{v} f = \int \mathrm{d}^3 v \, [\boldsymbol{v}_{\parallel} + \boldsymbol{v}_{\mathrm{d0}}] \bar{f} - \nabla \times \left(\frac{\boldsymbol{b}}{2\Omega} \int \mathrm{d}^3 v \, \bar{f} v_{\perp}^2 \right), \tag{3.27}$$

which contains an additional divergence-free term compared to (3.24). This term represents the magnetization flow due to the gyration of the particles around the guiding-centers, given by the $-\boldsymbol{\rho} \cdot \nabla \bar{f}$ term in (3.23). This form of the fluxes is well-known from local theory [42]; the only difference in the global theory is the ordering of specific terms. In particular, Ref. [78] shows that, to $\mathcal{O}(\delta v_T n)$, the sharp ψ gradients in g gives a new contribution to the divergenceless magnetization flux, while the $\boldsymbol{E} \times \boldsymbol{B}$ drift acting on g contributes to the poloidal fluxes.

Although the divergence-free term is of interest for calculating the fluxes within flux-surfaces, it does not directly contribute to the total radial transport – as follows from applying Gauss' theorem to the volume $V(\psi)$ bounded by that flux-surface ψ. Thus, the fluxes as implicitly defined by (3.24)–(3.26), are sufficient for calculating the total radial fluxes.

Moment equations directly involving these total radial fluxes are obtained by taking the flux-surface average of (3.24)–(3.26), and using the (2.74) property of the flux-surface average. For (3.24), this results in

$$\frac{1}{V'}\frac{\mathrm{d}}{\mathrm{d}\psi}\left(V'\langle\boldsymbol{\Gamma}\cdot\nabla\psi\rangle\right) = \left\langle\int \mathrm{d}^3v\, S\right\rangle. \tag{3.28}$$

This equation tells us that for $V'\langle\boldsymbol{\Gamma}\cdot\nabla\psi\rangle$ to vary radially – which would naturally occur as a consequence of the sharp radial variation we have allowed in g – sources are needed.

Physically, this result means that the sharp gradients observed in the pedestal will drive fluxes that are incompatible with steady-state collisional transport in the absence of sources, which is why we introduced sources in (3.16).

This incompatibility of steady-state assumptions and radially-global transport is also observed in gyrokinetic modeling of plasma turbulence [80], where one typically adds sources either to match physical sources in experiments (referred to as *flux-driven* simulations), or to make the profiles remain close to the experimentally observed profiles (known as *profile-driven* simulations) [81]. The latter approach is used in this work; an argument for this approach can be made as follows:

Experimentally observed steady-state profiles are necessarily consistent with the physical total fluxes and sources. If the modeled fluxes are not consistent, there must be other, unmodeled contributions to the flux such that the total flux respects the conservation laws, i.e., for particles

$$\begin{aligned} &\nabla\cdot(\boldsymbol{\Gamma}+\boldsymbol{\Gamma}_{\text{unmodeled}}) = S_{\text{physical}} \\ \Longrightarrow\ &\nabla\cdot\boldsymbol{\Gamma} = S_{\text{physical}} - \nabla\cdot\boldsymbol{\Gamma}_{\text{unmodeled}} \equiv S_{\text{effective}}, \end{aligned} \tag{3.29}$$

where S_{physical} is the physical source. From this equation, we can define an effective source-term given by the divergence of the unmodeled fluxes combined with the physical source. If the model for $\boldsymbol{\Gamma}$ does not depend on the unmodeled fluxes, solving for the sources needed for a consistent steady-state is equivalent to solving for the physical sources combined with the divergence of the unmodeled fluxes.

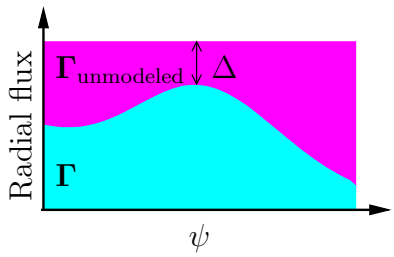

Figure 3.1: Unmodeled and modeled radial steady-state fluxes, for positive unmodeled fluxes and no physical sources. The difference between the maximum of the modeled fluxes and the total fluxes is indicated by Δ.

We will discuss how the effective sources are solved for in this work in the next section, where we describe how we numerically solve (3.16) for both g and S. Regardless of the solution method, a general issue with this approach may be noted, namely that the total flux is not determined. For the radial flux, the situation is illustrated in Figure 3.1 for the case of no physical sources, so that any radial gradient in the modeled radial flux must be balanced by the effective sources, here corresponding to a change in the unmodeled fluxes.

As the typical transport in tokamak plasmas is turbulent, a natural candidate for the unmodeled fluxes in our collisional transport model is the turbulent flux. In the pedestal, turbulence is decreased, while the sharp gradients cause the collisional transport to increase, which suggests a picture similar to Figure 3.1. If the unmodeled, radial turbulent fluxes are positive – as is typically the case for the turbulent heat flux – the peak value of the modeled collisional flux gives the best approximation to the total flux (with the error indicated by Δ in Figure 3.1). Furthermore, if the turbulent flux is small – as is suggested by the sometimes good agreement between collisionally modeled and experimental fluxes [28, 29, 32] – the error in this approximation will be small. Exact estimation of these errors would require radially-global turbulence simulations, which are beyond the scope of this work.

3.3 The PERFECT code

The PERFECT code solves discretized versions of either the local time-independent linearized DKE (3.17) or the global equation (3.16), taking

the zeroth order density, temperature and electrostatic potential as inputs and returning (moments of) g and the sources S as outputs.

In the global equation, the sources are solved for alongside g, typically by demanding that the flux-surface averages of the perturbed density and pressure are zero[2]

$$\begin{aligned} \left\langle \int \mathrm{d}^3 v\, g \right\rangle &= 0, \\ \left\langle \int \mathrm{d}^3 v\, v^2 g \right\rangle &= 0. \end{aligned} \tag{3.30}$$

This provides two ψ-dependent constraints for each species, which allows us to solve for the ψ-dependence of two kinds of sources – typically taken to be heat and particle sources in PERFECT. The velocity and θ dependence of the sources can be specified by the user; the former differentiates particle from heat sources. PERFECT allows for flexibility in specifying sources, and (3.30) can be supplemented or replaced with other constraints on g. For simulations with zero radial current – which is a practical requirement for confinement, see the discussion under (2.76) – we use an additional unknown momentum source with a prespecified species dependence to balance the additional constraint on the current.

Equation (3.30) also makes it easier to specify the zeroth-order Maxwellian from experimental data, as it implies that the density and temperature in the Maxwellian should correspond to the flux-surface averages of those quantities.

Apart from sources, the solution of the global equation is further complicated by the need to apply radial boundary conditions to the problem. PERFECT has the flexibility to apply three alternative conditions: Dirichlet boundary conditions $g(\psi_1) = g_{\mathrm{local}}(\psi_1)$ or $g(\psi_1) = 0$, or Neumann $\boldsymbol{v}_{\mathrm{d0}} \cdot \nabla g = 0$. These are applied at the boundaries where radially drifting particles enter the domain.

Rather than the W_0 and μ used to derive the DKE in the previous section, PERFECT uses $x = v/v_T$ and $\xi = v_\parallel/v$, which allows for a more convenient representation of the full linearized Fokker-Planck collision operator. The discretization of the problem is done by finite difference in ψ and θ, a Legendre polynomial expansion in ξ and by using spectral collocation in x [72].

[2]Note that g and f_1 have the same flux-surfaced averaged density and pressure, since $\langle \Phi_1 \rangle = 0$.

With this discretization, the global DKE (3.16) and the constraints (3.30) – and also the local DKE (3.17) without constraints – can be written as a matrix inversion problem. In PERFECT, this problem is solved using PETSc's Krylov solver [82] with preconditioners based on simplified forms of the problem, generated by, for example, dropping off-diagonal terms.

Factorization of the preconditioner matrix is typically the lengthiest part of the computation, and the often large size of the matrix means that PERFECT needs several hundred gigabytes of memory to solve the global equation at realistic resolutions. Depending on the tolerance requirement of the Krylov solver, numerous Krylov iterations may also be needed to obtain a solution.

Once the distribution is obtained, PERFECT calculates the fluxes described in the previous section as outputs. In Chapter 5, we summarize results obtained by applying PERFECT to a range of problems related to neoclassical pedestal transport, which formed the basis for Paper A, Paper B, and Paper C.

Chapter 4

Transport of highly-charged impurities

The transport of highly-charged impurities is a concern in any magnetic confinement system, as highly-charged impurities cannot be allowed to accumulate in the center of the plasma. It is also theoretically challenging, as their high charge makes them sensitive to small variations in electrostatic potential that is of little importance to describe the behaviour of the bulk hydrogen ions and electrons.

The importance of studying impurity transport was realized already in the early days of fusion research [83], and the effects of highly-charged impurities developing density variations along the magnetic field-lines was investigated in the late 1970's [84, 85]. A calculation of the self-consistent variation of impurities along field-lines due to friction, electrostatic potential and centrifugal forces in tokamaks may be found in Ref. [35]. These effects are not only important because they affect the self-consistent distribution of impurities, but they also allow for new methods of affecting the transport of impurities by manipulating the electrostatic potential in the plasma [86], which can be done by changing how the plasma is heated [87].

All the above studies were conducted for tokamaks. Recently, these effects have attracted an interest in the stellarator community [36, 37]. This chapter describes an analytic derivation of the transport of highly-charged impurities in the *mixed-collisionality regime*, adapted from Ref. [88] – see also Ref. [69] for an alternative derivation.

4.1 Highly-charged impurities

For highly-charged impurities, $Z \gg 1$ (where Z here refers to the impurity charge number, and the bulk ions are assumed to be singly charged), even the lowest order Maxwell-Boltzmann distribution (2.62) gives a density that varies on the flux-surface, through the $\mathrm{e}^{-\frac{Ze\Phi}{T}}$ term. To be explicit, we write the potential as

$$\Phi = \langle \Phi \rangle + \tilde{\Phi}, \tag{4.1}$$

where $\tilde{\Phi}$ is the part of Φ that varies on the flux-surface, and $\langle \Phi \rangle$ is the flux-surface average of the potential. In order to be able to neglect the flux-surface variation of Φ for the bulk hydrogen ions and electrons, we assume $\tilde{\Phi} \sim \frac{1}{Z} \langle \Phi \rangle$ so that $e\tilde{\Phi}/T$ is small in Z^{-1}.

As collisionality scales with Z^2, highly-charged impurities can be collisional even though the bulk-ions are in a low-collisionality regime. This is the case in the *mixed-collisionality regime*. The collisional impurities are thus Maxwellian also to higher-order, and we can use the fluid-equations (2.42)-(2.44) for the impurities with no further kinetic information.

For a Maxwellian impurity in steady-state, the equations for particle (2.42) and momentum conservation (2.43) reduce to

$$\nabla \cdot \boldsymbol{\Gamma}_z = 0, \tag{4.2}$$

$$\nabla p_z - Ze \left(n_z \boldsymbol{E} + \boldsymbol{\Gamma}_z \times \boldsymbol{B} \right) = \boldsymbol{F}_c, \tag{4.3}$$

while the energy conservation equation (2.44) implies that the impurities and main ions have equilibrated to the same temperature $T_z = T_i = T(\psi)$, which is a flux-function.

From (4.3), we obtain the average radial flux of impurities by projecting the equation onto $\boldsymbol{B} \times \nabla\psi$ and performing a flux-surface average

$$Ze \langle \boldsymbol{\Gamma}_z \cdot \nabla\psi \rangle = Ze \langle \boldsymbol{\Gamma}_z \cdot \nabla\psi \rangle^{\mathrm{NC}} + Ze \langle \boldsymbol{\Gamma}_z \cdot \nabla\psi \rangle^{\mathrm{C}}, \tag{4.4}$$

$$\langle \boldsymbol{\Gamma}_z \cdot \nabla\psi \rangle^{\mathrm{NC}} \equiv - \langle n_z \boldsymbol{B} \times \nabla\psi \cdot \nabla\Phi \rangle - \frac{T}{Ze} \langle \boldsymbol{B} \times \nabla\psi \cdot \nabla n_z \rangle, \tag{4.5}$$

$$\langle \boldsymbol{\Gamma}_z \cdot \nabla\psi \rangle^{\mathrm{C}} \equiv \langle \boldsymbol{B} \times \nabla\psi \cdot \boldsymbol{F}_c \rangle. \tag{4.6}$$

Here $\langle \boldsymbol{\Gamma}_z \cdot \nabla\psi \rangle^{\mathrm{C}}$ is the classical transport, caused directly by perpendicular friction; $\langle \boldsymbol{\Gamma}_z \cdot \nabla\psi \rangle^{\mathrm{NC}}$ is the neoclassical transport, caused by the electric fields and pressure in the $\boldsymbol{B} \times \nabla\psi$-direction. The neoclassical transport is often expressed in terms of parallel friction. To show the

relation between neoclassical transport and parallel friction, we take the $\boldsymbol{B}$ projection of (4.3), resulting in

$$TBn_z\nabla_\parallel\left(\ln n_z+\frac{Ze}{T}\Phi\right)=F_{c\parallel,z}. \tag{4.7}$$

To proceed, we introduce the quantity w, which is defined through the magnetic differential equation

$$\boldsymbol{B}\cdot\nabla(n_z w)=-\boldsymbol{B}\times\nabla\psi\cdot\nabla\left(\frac{n_z}{B^2}\right). \tag{4.8}$$

Multiplying (4.7) by w and flux-surface averaging, the relation (2.75) allows us to move the parallel derivative to $n_z w$ by partial integration, at which point (4.8) lets us translate the parallel derivative into a derivative in the $\boldsymbol{B}\times\nabla\psi$-direction. Then, (2.76) and another partial integration yields

$$\begin{aligned}Ze\left\langle\boldsymbol{\Gamma}_z\cdot\nabla\psi\right\rangle^{\mathrm{NC}}=&-Ze\left\langle n_z\boldsymbol{B}\times\nabla\psi\cdot\nabla\Phi\right\rangle-T\left\langle\boldsymbol{B}\times\nabla\psi\cdot\nabla n_z\right\rangle\\=&Ze\left\langle wBF_{c\parallel,z}\right\rangle,\end{aligned} \tag{4.9}$$

showing that the neoclassical transport indeed is related to parallel friction, and that wB acts as a weighting function for integrating up the neoclassical transport from the parallel friction. For cases where n_z is constant on the flux-surface, w reduces to the geometric function u

$$\boldsymbol{B}\cdot\nabla u=-\boldsymbol{B}\times\nabla\psi\cdot\nabla\left(\frac{1}{B^2}\right). \tag{4.10}$$

For magnetic fields with toroidal symmetry, $w=-IB^{-2}$ up to an integration constant, where the flux-function I is related to toroidal magnetic field B_t and major radius R through $I=RB_t$.

Although (4.9) shows mathematically how parallel friction causes neoclassical transport, it is non-trivial to evaluate the parallel friction on the impurities. Since the impurities cannot transfer momentum to themselves, the friction force is set by collisions with bulk ions and electrons, where the contribution from the more massive ions dominates, see (2.34), so that

$$\boldsymbol{F}_{c,z}\approx\boldsymbol{F}_{c,zi}=-\boldsymbol{F}_{c,iz}. \tag{4.11}$$

The last step results from the momentum conservation property of the collision operator, (2.30). Furthermore, since the bulk ions are in the low-collisionality regime, the friction force is typically smaller than the

force due to the electric field in the parallel momentum equation (4.7). We can quantify this smallness by introducing the parameter [34]

$$\Delta \equiv Z^2 \epsilon \hat{\nu}_{ii} \ll 1. \tag{4.12}$$

This is convenient, since it allows us evaluate the friction force to order Δ^1 from n_z to order Δ^0, which will be sufficient to evaluate the transport.

To order Δ^0, the impurity density merely responds to the electric field, reproducing the zeroth-order result in the ϵ expansion (2.62)

$$n_{z0} = N_z \mathrm{e}^{-Ze\tilde{\Phi}/T} = \int \mathrm{d}^3 v \, f_{Mz}, \tag{4.13}$$

where we have defined a new pseudo-density N_z, which is related to pseudo-density η in previous sections by

$$N_z \equiv \eta_z \mathrm{e}^{-Ze\langle\Phi\rangle/T}. \tag{4.14}$$

The equivalence of the Δ and ϵ expansion-results to this order follows from the fact that $R_{z\|} = 0$ if both the ions and the impurities are Maxwell-Boltzmann distributed (2.62).

To evaluate the impurity-ion friction force due to the above n_{z0} (4.13), we require parts of f_{i1} in the low-collisionality regime, determined by (2.67)-(2.69). When the impurities are trace, the effect of the impurities on f_{i1} can be neglected, so that f_{i1} calculated for a pure plasma can be used [89]. The non-trace impurity limit is more complicated; for impurities which are constant on the flux-surface ($\tilde{\Phi} = 0$) the required parts of f_{i1} were obtained in Ref. [90]. These results can be generalized to the case of impurities varying on the flux-surface ($\tilde{\Phi} \neq 0$) by essentially repeating the previous calculations [88]. These calculations all rely on the mass-ratio expanded collision operator (2.32) to make them analytically tractable, using the fact that highly-charged impurities are much heavier than the bulk hydrogen ions. The resulting impurity flux can be written

$$\frac{\langle \mathbf{\Gamma}_z \cdot \nabla\psi \rangle^{\mathrm{NC}}}{\langle n_{z0} \rangle} = D_{\Phi}^{\mathrm{NC}} \frac{e}{T_i} \frac{\mathrm{d}\langle\Phi\rangle}{\mathrm{d}\psi} - \frac{1}{Z} D_{N_z}^{\mathrm{NC}} \frac{\mathrm{d}\ln N_z}{\mathrm{d}\psi} - D_{n_i}^{\mathrm{NC}} \frac{\mathrm{d}\ln n_i}{\mathrm{d}\psi} - D_{T_i}^{\mathrm{NC}} \frac{\mathrm{d}\ln T_i}{\mathrm{d}\psi}, \tag{4.15}$$

where the transport coefficients D^{NC} are

$$D_{\Phi}^{\mathrm{NC}} = - D_{N_z} - D_{n_i} \tag{4.16}$$

$$D_{N_z}^{\mathrm{NC}} = \frac{m_i n_i T_i}{Ze^2 \langle n_{z0} \rangle n_{z0} \tau_{iz0}} \left[\langle n_{z0} w_0^2 B^2 \rangle - \langle n_{z0} w_0 B^2 \rangle \frac{\langle w_0 B^2 \rangle}{\langle B^2 \rangle} \right. \tag{4.17}$$
$$\left. + \frac{\frac{\langle n_{z0} w_0 B^2 \rangle}{\langle B^2 \rangle} \left\langle \frac{B^2}{n_{z0}} \right\rangle - \langle w_0 B^2 \rangle}{\left\langle \frac{B^2}{n_{z0}} (1 - c_4 \alpha) \right\rangle} \langle (1 - c_4 \alpha) w_0 B^2 \rangle \right]$$

$$D_{n_i}^{\mathrm{NC}} = - \frac{m_i n_i T_i}{Ze^2 \langle n_{z0} \rangle n_{z0} \tau_{iz0} Ze} \left[\langle n_{z0} w_0 u B^2 \rangle - \langle n_{z0} w_0 B^2 \rangle \frac{\langle u B^2 \rangle}{\langle B^2 \rangle} \right. \tag{4.18}$$
$$\left. + \frac{\frac{\langle n_{z0} w_0 B^2 \rangle}{\langle B^2 \rangle} \left\langle \frac{B^2}{n_{z0}} \right\rangle - \langle w_0 B^2 \rangle}{\left\langle \frac{B^2}{n_{z0}} (1 - c_4 \alpha) \right\rangle} \left(c_2 + \langle u B^2 \rangle [c_1 + 1] \right) \right]$$

$$D_{T_i}^{\mathrm{NC}} = \frac{m_i n_i T_i}{Ze^2 \langle n_{z0} \rangle n_{z0} \tau_{iz0}} \left[\frac{1}{2} \left(\langle n_{z0} w_0 u B^2 \rangle - \langle n_{z0} w_0 B^2 \rangle \frac{\langle u B^2 \rangle}{\langle B^2 \rangle} \right) \right. \tag{4.19}$$
$$\left. - \frac{\frac{\langle n_{z0} w_0 B^2 \rangle}{\langle B^2 \rangle} \left\langle \frac{B^2}{n_{z0}} \right\rangle - \langle w_0 B^2 \rangle}{\left\langle \frac{B^2}{n_{z0}} (1 - c_4 \alpha) \right\rangle} \left(c_3 - \frac{3}{2} c_2 - \langle u B^2 \rangle \left[c_1 (1.17 - 1) + \frac{1}{2} \right] \right) \right],$$

where the collision time is $\tau_{iz} = \frac{4}{3\sqrt{\pi}\nu_{iz}}$; $\alpha = Z^2 n_z / n_i$; and we have introduced the flux-surface constants c_1, c_2, c_3, and c_4, which depend on both magnetic geometry and the impurity density, and are defined in Ref. [88]. The zero subscript on w and τ_{iz} indicates that n_{z0} (4.13) are used instead of the exact n_z.

The transport coefficients (4.16)-(4.19) have several new features compared to the $\tilde{\Phi} = 0$ case – most notably, $D_\Phi \neq 0$, which means that a radial electric field can drive transport in the mixed-collisionality regime. The transport driven by the radial electric field grows quite rapidly with the amplitude of $\tilde{\Phi}$ [69, 88], which may be important in order to explain why stellarator experiments frequently observe accumulation of impurities when operating with inward electric field [15]. This electric field configuration is expected when the electron and ion temperatures are comparable [16], which is a preferred regime for future reactors [17].

The expression for the flux in (4.15) does not include the classical transport, which is normally smaller than the neoclassical flux. The classical flux can be readily calculated from the gyrophase varying part of f in (2.59). For the same mass-ratio expanded collision operator (2.32), the classical transport is calculated as the friction force resulting from the lowest-order gyrophase dependent f, resulting in

$$\begin{aligned}\langle \boldsymbol{\Gamma}_z \cdot \nabla\psi \rangle^{\mathrm{C}} \equiv & \frac{1}{Ze} \left\langle \frac{\boldsymbol{B} \times \nabla\psi}{B^2} \cdot \boldsymbol{F}_{c,z} \right\rangle \\ = & \frac{m_i n_i}{Z e n_z \tau_{iz}} \left\langle n_z \frac{|\nabla\psi|^2}{B^2} \right\rangle \frac{T_i}{e} \left[\frac{\mathrm{d}\ln n_i}{\mathrm{d}\psi} - \frac{1}{2}\frac{\mathrm{d}\ln T_i}{\mathrm{d}\psi} - \frac{1}{ZN_z}\frac{\mathrm{d}N_z}{\mathrm{d}\psi} \right].\end{aligned} \tag{4.20}$$

As was mentioned in Section 2.1.2, while the classical transport is usually small, it can be dominant for collisional impurities in certain stellarators. We can now quantify this statement by comparing (4.20) and (4.15). Taking the simple $\tilde{\Phi} = 0$ limit, we find the ratio of classical to neoclassical transport purely depends on the magnetic geometry

$$\frac{\langle \boldsymbol{\Gamma}_z \cdot \nabla\psi \rangle^{\mathrm{C}}}{\langle \boldsymbol{\Gamma}_z \cdot \nabla\psi \rangle^{\mathrm{NC}}} = \frac{\left\langle \frac{|\nabla\psi|^2}{B^2} \right\rangle \langle B^2 \rangle}{\left(\langle u^2 B^2 \rangle \langle B^2 \rangle - \langle u B^2 \rangle^2 \right)}. \tag{4.21}$$

This ratio can be rewritten in terms of the ratio of perpendicular and parallel current density,

$$\frac{\langle \boldsymbol{\Gamma}_z \cdot \nabla\psi \rangle^{\mathrm{C}}}{\langle \boldsymbol{\Gamma}_z \cdot \nabla\psi \rangle^{\mathrm{NC}}} = \frac{\langle j_\perp^2 \rangle \langle B^2 \rangle}{\left\langle j_\parallel^2 \right\rangle \langle B^2 \rangle - \langle j_\parallel B \rangle^2}. \tag{4.22}$$

which has been optimized to be large in the Helias line of stellarators, including Wendelstein 7-X[1]. As a result, collisional impurities in these stellarators can have a sizable ratio of classical to neoclassical transport.

The analytical classical to neoclassical ratio (4.22) is valid for the mixed-collisionality regime, for impurities with large masses compared to the bulk ions. These are the assumptions made in the analytical calculation that formed the basis of Paper D and Paper E. To investigate the ratio of classical to neoclassical fluxes at any collisionality regime, for the full Fokker-Planck collision operator (2.27), numerical calculations of the neoclassical fluxes are needed. In Paper F, we performed such calculations using the Sfincs code, which is described in the next section.

[1]The world's largest stellarator, operated by the Max Planck Institute of Plasma Physics at Greifswald, Germany.

4.2 The SFINCS code

The SFINCS code [91] solves the linearized radially-local drift-kinetic equation (2.63) for stellarator geometry. The lack of a symmetry direction in a general stellarator means that the equation is 4-dimensional, in the sense that the terms in the equation generally depend on four variables: ζ, θ, $x = v/v_T$ and $\xi = v_\parallel/v$. This makes the computational requirements comparable to those of the radially-global tokamak code PERFECT, which SFINCS was based on. SFINCS thus mostly uses the same numerical tools as PERFECT, including PETSc's Krylov solver.

Due to the higher computational costs, stellarator calculations have historically used simplified collision operators retaining only pitch-angle scattering [91], which SFINCS also supports for the sake of comparison. This simplified operator is adequate at low collisionality, but becomes inaccurate for highly-charged impurities, which typically have higher collisionality [92]. Pitch-angle scattering calculations are nevertheless routinely done for impurities due to their computational simplicity [93].

SFINCS also has the option to include the effects of variations in the electrostatic potential on the fluxes for any species. This is done by including the variation in the electrostatic potential, in SFINCS denoted by Φ_1, in the lowest order distribution function for all species. Here, Φ_1 is calculated through the quasi-neutrality equation, using $f_0 + f_1$ to calculate the density variation on the flux-surface

$$\sum_a Z_a \int \mathrm{d}^3 v (f_{a0} + f_{a1}) = 0, \tag{4.23}$$

where Φ_1 enters the equation through f_{a0}. This makes the equation nonlinear, due to the drift velocity multiplying ∇f_0 in (2.63). The resulting nonlinear equation is solved by using PETSc's implementation of Newton's method to reduce the nonlinear problem into a sequence of linear problems, which again are solved using PETSc's Krylov solver. The nonlinear problem thus requires an order of magnitude more computational time. To avoid performing such calculations, Paper F makes use of a small number of nonlinear SFINCS simulations, performed as part of a different study [37]. As described in Paper F, the calculation of the classical transport can be performed as a post-processing step to already existing SFINCS calculations.

Chapter 5

Summary of papers

In the previous chapters, we introduced a theoretical framework for studying neoclassical transport in tokamak pedestals and stellarators. In this chapter, we give an overview of the work we have done in this framework by summarizing the six attached papers. Papers A-C are concerned with tokamak pedestal transport as described in Chapter 3, while Papers D-F treat the collisional transport of highly-charged impurities in stellarators.

In Paper A we looked at changes in transport due to the presence of trace and non-trace nitrogen *impurities* in the pedestal. While impurities cannot be allowed to accumulate in the hot core of the plasma, they can also have beneficial effects. As an example of this, when the tokamak JET[1] switched from a carbon to a beryllium-tungsten ("ITER[2]-like") wall, there was a reduction in energy confinement [94–96]. This decrease in confinement was attributed to a reduction in the impurity content of the plasma as a result of the new wall, but previous confinement levels could sometimes be recovered by injecting nitrogen [95, 97].

To study this, we generated a density and electron temperature profile similar to experimental JET electron profiles (Figure 16 of Ref. [98]), and complemented this with model potential and ion temperature profiles designed to satisfy the assumptions of the global DKE: gentle T_i

[1] **J**oint **E**uropean **T**orus, the world's largest tokamak, hosted in the UK on behalf of EUROfusion.

[2] *ITER*: Latin for "the way", a tokamak currently being built in Cadarache, France, which upon its completion will be the largest tokamak to date.

variations – here based on the core T_e gradients – and electrostatic ion confinement.

As a result of the electron temperature pedestal, large electron particle fluxes developed both in and across flux-surfaces. These fluxes were well described by the local theory, due to the small orbit width of the electrons and the low flow of the ions, which otherwise could affect the electrons through collisions. Thus, the parallel current in these simulations were close to results from the local theory. This has implications for evaluating the performance of a tokamak reactor, as the poloidal magnetic field – which determines the orbit width – is set by this current. In addition, stronger parallel current can drive so-called peeling-modes unstable, which can drive the plasma away from a stable pedestal configuration and cause large intermittent heat fluxes [98–101].

For bulk and impurity ions, the global effects caused order unity relative modifications to ion heat and particle fluxes, with impurity particle fluxes even changing sign compared to the local results. These effects are not restricted to the pedestal region, but due to the radially global nature of these effects, they extend a distance into the near-pedestal core, and this distance was observed to scale with the orbit width of the species, as expected.

Furthermore, it was found that the momentum transport was strongly affected by the nitrogen seeding, which could imply that the confinement improvement due to nitrogen seeding might not be directly related to a reduction in heat flux, but due to a more efficient suppression of turbulence. The analysis in Paper A did not explicitly enforce intrinsic ambipolarity of the particle fluxes, and a non-zero radial current developed together with a significant radial flux of toroidal angular momentum. In Paper B, we showed that this non-zero radial neoclassical current can be replaced with a momentum source to yield a system consistent with steady-state. Even with this replacement, the radial momentum fluxes remained non-zero and qualitatively similar to those in the presence of the radial current.

In Paper B, we used similar input profiles as in Paper A to study pedestal flows in deuterium (D), helium (He) and mixed D-He plasmas. The aim of the study was to investigate whether the He flow is a suitable proxy for the D flow, since the latter is much more difficult to measure in experiments [102]. Specifically, we investigated to what extent the flow of He impurities in a bulk D plasmas is similar to the D flow, and

also if the He flow in bulk He plasma is similar to the D flow in a bulk D plasma.

We found that the flow of He impurities in a D bulk plasma can be quite similar to those in a bulk He plasma – i.e. that the species role as bulk or impurity was not the dominant factor in our study. Specifically, the extremum values in outboard ($\theta = 0$) and inboard ($\theta = \pi$) poloidal flows were within 0.3 km/s absolute and 15% relative difference, which is within current experimental uncertainties in flow measurements [103, 104]. Likewise, the extremum values of the poloidal D flows in the bulk and impurity scenario were within 0.5 km/s of each other.

On the other hand, the difference in poloidal flows between the species were significant, around 10 km/s, which indicates that He flows may not be a suitable proxy for D flows. Despite difference in magnitude, the shape of the D and He flow structures in the radial-poloidal plane were qualitatively similar to each other, if the thermal orbit width of the species is interpreted as setting the radial scale of these structures, and this difference is compensated for.

Furthermore, as the divergence of the radial fluxes can not be neglected in the global theory, since the non-adiabatic response g varies on the orbit-width scale, there is a potential for interactions between radial and poloidal fluxes. As a result, radial-poloidal structures in the particle flux can form near the pedestal. As the fluxes are not divergence free on a flux-surface – as assumed in the local theory – the poloidal flow coefficient[3] is not a flux-function, and can even change sign between inboard and outboard side. Thus, changes in the sign of the poloidal flow on a flux-surface could potentially be an experimental signature of global effects.

In Paper C, we investigated isotopic effects in the pedestal. The isotope effect is a phenomenon where the ion heat fluxes do not scale with the square-root of the ion mass [105–108], which would be the expected scaling from collisional transport and some models for plasma turbulence, such as *ion-temperature gradient* modes [109]. The isotope effect is typically seen to be stronger for H-mode plasmas [110, 111], and is thus an interesting topic for radially-global studies. Global effects tend to reduce the ion heat flux in the pedestal compared to locally predicted

[3]The poloidal flow coefficient, k_p, is essentially the proportionality coefficient between temperature gradient and poloidal flow V_p, with some additional geometric factors: $V_p = k_p B_p B_t R/(e\langle B^2\rangle)\mathrm{d}T/\mathrm{d}\psi$.

values, and these effects are stronger for heavier isotopes due to their wider orbit-widths.

We also investigated the extent to which global corrections to local results can be predicted by experimentally measurable density pedestal parameters: reciprocal pedestal width over orbit width, relative pedestal density drop and logarithmic gradient times orbit width. The impact of global effects typically increase with all these parameters, and showed signs of saturation for higher values. For fixed width and density at the last-closed flux-surface, the global conductive and convective heat fluxes become less sensitive to the pedestal gradient as it increases, so that the difference between local and global convective and conductive fluxes even may change sign. The trends for the sum of conductive and convective heat fluxes were in general too complicated to give clear predictions: Simple empirical models based on polynomials of low degree gave large residuals (and were thus not included in the published paper).

To summarize the pedestal work: we found that radially global effects can introduce order unity modifications to particle and heat fluxes, which extend into the near-pedestal core; the fluxes are no longer divergence free on flux-surfaces; the ambipolarity of the particle fluxes needs to be enforced, and momentum transport appears at lower order and is sensitive to impurities.

Starting in Paper D, we changed focus and considered the transport of a collisional impurity species in an otherwise pure stellarator plasma, in the mixed-collisionality regime. In previous stellarator studies, it was found that the impurity transport of a collisional impurity is independent of the radial electric-field [90, 112, 113]. This is generally not the case in stellarators, and goes against the conventional wisdom that an inward radial electric-field transports impurities into the plasma [92]. However, when we generalized the previous mixed-collisionality regime calculation in Ref. [90, 113] to account for flux-surface variation in the impurity density, we found that the impurity transport once again depends on the radial electric-field, and often leads to impurity transport in the direction of the electric field.

Even so, under rare circumstances, an inward radial electric field was found to transport impurities outwards. These results were also found independently by Calvo et al. [69], and may be applicable to preventing impurities from accumulating in stellarators. This potential application inspired the optimization effort underlying Paper E. In addition,

we derived the ratio between classical and neoclassical flux (4.21) in the mixed-collisionality regime, which strongly indicated that classical transport of a high-collisionality impurity is relevant in Helias-type optimized stellarators such as Wendelstein 7-X (W7-X). This was further studied in Paper F.

In Paper E, we applied the expression for the transport coefficients of impurities derived in Paper D to minimize the impurity *peaking factor* with respect to the impurity variation on the flux-surface. The impurity peaking factor is defined as minus the logarithmic impurity pseudo-density gradient, $-\mathrm{d}\ln N_z/\mathrm{d}\psi$, that causes the radial impurity flux $\langle \mathbf{\Gamma}_z \cdot \nabla\psi \rangle$ to be zero, given that all other profiles are fixed. The peaking-factor determines the steady-state profile of impurities – as set by the collisional transport and ignoring any source-term – and minimizing the peaking-factor minimizes the amount of impurities in the middle of the plasma. For a W7-X *standard case* (which refers to the choice of magnetic field configuration) [114], the minimization procedure found impurity variations that reduce the central impurity density by the factor 0.89^Z, compared to the case when the impurity density is constant on the flux-surface. For an LHD[4] impurity hole case, the optimal reduction was even more significant (0.75^Z). This results in a large reduction for large Z. Furthermore, as these reductions are compared to a constant n_z, the effect may be even more significant when comparing to unoptimized n_z variations, as most n_z variations appear to be unfavorable for the purpose of expelling impurities.

This study was merely concerned with finding the optimal impurity density variation, and did not consider whether or how such optima can be achieved in experiments. However, an independent simulation study by Yamaguchi & Murakami [38] on the influence of neutral-beam injection (NBI) heating on the electrostatic potential variation indicates that impurity density variations qualitatively similar to our LHD optimum could be achieved by neutral-beam injection perpendicular to the magnetic field. Yamaguchi & Murakami also found a reduction in impurity accumulation under these conditions, using numerical simulations to evaluate the neoclassical transport.

In Paper F, we looked further into the ratio of neoclassical and classical impurity transport in stellarators, by considering how this ratio

[4] **L**arge **H**elical **D**evince, a stellarator in Japan.

varies with collisionality. To calculate the neoclassical impurity transport for any collisionality, we used the SFINCS drift-kinetic solver [91]. In order to have an expression for the classical transport that is directly comparable to the neoclassical transport calculated with SFINCS, we generalized the classical calculation in Paper D to use the full Fokker-Planck collision operator (2.27), using the Braginskii-matrix method (see, for example, Ref. [115]). For a W7-X standard configuration with a carbon impurity, we found that the classical transport is not only important for highly-collisional impurities, but the classical transport coefficients become comparable to the neoclassical already for impurity self-collisionalities $\hat{\nu}_{\mathrm{CC}} \sim 0.1$–$1$. As the classical transport is only dominant for collisional impurities in stellarators optimized for low parallel current, it is also of interest to compare this to the LHD impurity hole case, where the classical transport coefficients are smaller than the neoclassical even at high collisionality. The classical transport can still be significant compared to the neoclassical in a narrow collisionality range where the neoclassical coefficients change sign.

The classical transport can be thought of as an irreducible minimum of collisional transport, as it cannot be optimized away by optimizing the magnetic field to better confine the drift orbits, but merely depends on the magnetic field strength. Thus, the fact that optimized stellarators such as W7-X have classical levels of impurity transport indicates that the overall collisional transport of impurities is low. Hence, other transport channels – such as turbulence – could be expected to play a large role in the transport of these impurities. This picture is supported by recent experimental studies [93, 116], where iron impurity transport coefficients about a hundred times larger than those predicted by neoclassical theory were measured. This is a novel situation, as the typical unoptimized stellarator had such strong neoclassical transport as to make turbulent transport irrelevant [117].

Thus, further studies into impurity transport in stellarators will likely need to take turbulence into account. A capability to perform such computations already exist [118, 119], but the simulations are computationally expensive and are thus not routinely performed. Thus, predicting the impurity transport in Wendelstein 7-X is likely to remain a challenge in the near future.

Summary and outlook We theoretically investigated collisional transport in tokamak pedestals and the collisional transport of heavy impu-

rities in stellarators, using models based on the drift-kinetic framework.

In tokamak pedestals, we found that global effects can introduce order unity changes to heat and particle fluxes. In the global theory, momentum transport appears at a lower order in the perturbation expansion, and is sensitive to impurities in the plasma. These effects also extend into the near-pedestal core. The fluxes are no longer divergence free within the flux-surfaces, which modifies the toroidal and poloidal flows.

Concerning impurity transport in stellarators, we found that electrostatic potential variations along the field-line cause the transport of collisional impurities to become sensitive to the radial electric field. These variations often increase impurity accumulation for cases with inward radial electric fields, but can in some circumstances lead to impurity expulsion. We have found electrostatic potential variations optimized to reduce the accumulation of impurities. These optima are similar to the variations seen in simulations of neutral beam heating in the LHD, when the beam is perpendicular to the magnetic field [38].

Future improvements to the pedestal modeling capabilities of PERFECT can be considered. There still remain questions regarding the basic equation system in PERFECT: The global DKE (3.16) combined with the constraints (3.30) and boundary conditions. As was mentioned in Section 3.1, the global DKE is not consistent without time-dependence or an effective source-term. This suggests that pedestal neoclassical transport is best studied in combination with another transport mechanism. For example, by performing full-f pedestal turbulence simulations, it may be possible to extract a physics based form for the sources in PERFECT.

For the stellarator impurity transport part of this thesis, an obvious next step would be to compare the analytic expression for the neoclassical impurity flux to SFINCS simulations using the same electrostatic potential variation along the field line in both calculations. An exciting next step would be to experimentally compare how impurities accumulate with perpendicular or parallel neutral beam injection in LHD. More generally, our analytical results could be used to investigate how to heat the plasma in order to reduce impurity accumulation in other machines.

To put the collisional transport discussed in this thesis in a broader context, we note that there are other relevant transport mechanisms: turbulence in both pedestals and stellarators [93, 120], regions with stochastic magnetic field in stellarators [121], transient processes in tokamak pedestals [122], can all cause transport. It remains a great chal-

lenge, both computationally and conceptually, to combine these different mechanisms. This is the computational frontier of plasma physics. Improving our understanding of the different mechanisms and their interactions is key to integrating all these processes, with the ultimate aim of self-consistently describing the transport in a fusion reactor.

To conclude, collisional transport is one important piece in the puzzle of plasma transport. The work done in this thesis has given us a better understanding of this piece, which will allow us to better put together the picture of transport necessary to build and control a fusion reactor.

Bibliography

[1]R. Clausius and T. Hirst, *The mechanical theory of heat: with its applications to the steam-engine and to the physical properties of bodies* (J. Van Voorst, 1867).

[2]L. Boltzmann and B. McGuinness, *Theoretical physics and philosophical problems: selected writings*, Vienna Circle Collection (Springer Netherlands, 2012).

[3]W. Huang et al., "The AME2016 atomic mass evaluation (I). evaluation of input data; and adjustment procedures", Chinese Physics C **41**, 030002 (2017).

[4]M. Wang et al., "The AME2016 atomic mass evaluation (II). tables, graphs and references", Chinese Physics C **41**, 030003 (2017).

[5]M. P. Fewell, "The atomic nuclide with the highest mean binding energy", American Journal of Physics **63**, 653–658 (1995).

[6]R. H. Cyburt et al., "Big bang nucleosynthesis: present status", Rev. Mod. Phys. **88**, 015004 (2016).

[7]J. P. Conner, T. W. Bonner, and J. R. Smith, "A study of the $H^3(d,n)He^4$ reaction", Phys. Rev. **88**, 468–473 (1952).

[8]W. R. Arnold et al., "Cross sections for the reactions $D(d,p)T$, $D(d,n)He^3$, $T(d,n)He^4$, and $He^3(d,p)He^4$ below 120 keV", Phys. Rev. **93**, 483–497 (1954).

[9]R. Miller, *An introduction to the physics of intense charged particle beams* (Springer US, 2012).

[10]D. Keefe, "Inertial confinement fusion", Annual Review of Nuclear and Particle Science **32**, 391–441 (1982).

[11]H. Antia, A. Bhatnagar, and P. Ulmschneider, *Lectures on solar physics*, Lecture Notes in Physics (Springer Berlin Heidelberg, 2003).

[12]L. Spitzer, "The stellarator concept", The Physics of Fluids **1**, 253–264 (1958).

[13]P. Helander, "Theory of plasma confinement in non-axisymmetric magnetic fields", Reports on Progress in Physics **77**, 087001 (2014).

[14]P. Helander, L.-G. Eriksson, and F. Andersson, "Runaway acceleration during magnetic reconnection in tokamaks", Plasma Physics and Controlled Fusion **44**, B247–B262 (2002).

[15]R. Burhenn et al., "On impurity handling in high performance stellarator/heliotron plasmas", Nuclear Fusion **49**, 065005 (2009).

[16]M. Yokoyama et al., "Core electron-root confinement (CERC) in helical plasmas", Nuclear Fusion **47**, 1213–1219 (2007).

[17]A. Sagara, Y. Igitkhanov, and F. Najmabadi, "Review of stellarator/heliotron design issues towards MFE DEMO", Fusion Engineering and Design **85**, Proceedings of the Ninth International Symposium on Fusion Nuclear Technology, 1336–1341 (2010).

[18]H. Bolt et al., "Plasma facing and high heat flux materials – needs for ITER and beyond", Journal of Nuclear Materials **307-311**, 43–52 (2002).

[19]J. W. Connor and H. R. Wilson, "Survey of theories of anomalous transport", Plasma Physics and Controlled Fusion **36**, 719 (1994).

[20]F. Jenko, W. Dorland, and G. W. Hammett, "Critical gradient formula for toroidal electron temperature gradient modes", Physics of Plasmas **8**, 4096–4104 (2001).

[21]P. Mantica et al., "Experimental study of the ion critical-gradient length and stiffness level and the impact of rotation in the JET tokamak", Phys. Rev. Lett. **102**, 175002 (2009).

[22]R. Balescu, *Aspects of anomalous transport in plasmas*, Series in Plasma Physics (CRC Press, 2005).

[23]F. Wagner et al., "Regime of improved confinement and high beta in neutral-beam-heated divertor discharges of the ASDEX tokamak", Phys. Rev. Lett. **49**, 1408–1412 (1982).

[24]F. Wagner, "A quarter-century of H-mode studies", Plasma Physics and Controlled Fusion **49**, B1 (2007).

[25]F. Wagner et al., "Development of an edge transport barrier at the H-mode transition of ASDEX", Phys. Rev. Lett. **53**, 1453–1456 (1984).

[26]ITER Physics Expert Group on Confinement and Transport, ITER Physics Expert Group on Confinement Modelling and Database, and ITER Physics Basis Editors, "Chapter 2: plasma confinement and transport", Nuclear Fusion **39**, 2175 (1999).

[27]H. Zohm et al., "On the physics guidelines for a tokamak DEMO", Nuclear Fusion **53**, 073019 (2013).

[28]J. Connor et al., "A review of internal transport barrier physics for steady-state operation of tokamaks", Nuclear Fusion **44**, R1 (2004).

[29]H. Urano et al., "Reduced heat transport between edge-localized-mode bursts at low collisionality and small poloidal Larmor radius", Phys. Rev. Lett. **95**, 035003 (2005).

[30]K. D. Marr et al., "Comparison of neoclassical predictions with measured flows and evaluation of a poloidal impurity density asymmetry", Plasma Physics and Controlled Fusion **52**, 055010 (2010).

[31]E. Viezzer et al., "Evidence for the neoclassical nature of the radial electric field in the edge transport barrier of ASDEX Upgrade", Nuclear Fusion **54**, 012003 (2014).

[32]E. Viezzer et al., "Investigation of inter-ELM ion heat transport in the H-mode pedestal of ASDEX Upgrade plasmas", Nuclear Fusion **57**, 022020 (2017).

[33]D. Meade, "Effect of high-Z impurities on the ignition and lawson conditions for a thermonuclear reactor", Nuclear Fusion **14**, 289–291 (1974).

[34]P. Helander, "Bifurcated neoclassical particle transport", Physics of Plasmas **5**, 3999–4004 (1998).

[35]T. Fülöp and P. Helander, "Nonlinear neoclassical transport in a rotating impure plasma with large gradients", Physics of Plasmas **6**, 3066–3075 (1999).

[36]J. García-Regaña et al., "Electrostatic potential variation on the flux surface and its impact on impurity transport", Nuclear Fusion **57**, 056004 (2017).

[37]A. Mollén et al., "Flux-surface variations of the electrostatic potential in stellarators: impact on the radial electric field and neoclassical impurity transport", Plasma Physics and Controlled Fusion **60**, 084001 (2018).

[38]H. Yamaguchi and S. Murakami, "Simulation study of electrostatic potential generated by NBI and its effect on the neoclassical transport of carbon impurity ions in LHD", IAEA Fusion Energy Conference preprints, Gandhinagar, India, TH/P6–29 (2018).

[39]M. Kruskal, "Asymptotic theory of hamiltonian and other systems with all solutions nearly periodic", Journal of Mathematical Physics **3**, 806–828 (1962).

[40]A. Baños, "The guiding centre approximation in lowest order", Journal of Plasma Physics **1**, 305–316 (1967).

[41]R. Hastie, J. Taylor, and F. Haas, "Adiabatic invariants and the equilibrium of magnetically trapped particles", Annals of Physics **41**, 302–338 (1967).

[42]R. D. Hazeltine and J. D. Meiss, *Plasma confinement*, Dover Books on Physics (Dover Publications, 2013).

[43]M. Kruskal, *The gyration of a charged particle*, tech. rep. NYO-7903; PM-S-33 (Project Matterhorn, Princeton University, 1958).

[44]A. Lenard, "Adiabatic invariance to all orders", Annals of Physics **6**, 261–276 (1959).

[45]C. S. Gardner, "Adiabatic invariants of periodic classical systems", Phys. Rev. **115**, 791–794 (1959).

[46]R. G. Littlejohn, "Variational principles of guiding centre motion", Journal of Plasma Physics **29**, 111–125 (1983).

[47]R. D. Hazeltine and F. Waelbroeck, *The framework of plasma physics*, Frontiers in physics (Avalon Publishing, 2004).

[48]R. J. Akers et al., "Transport and confinement in the Mega ampère spherical tokamak (MAST) plasma", Plasma Physics and Controlled Fusion **45**, A175–A204 (2003).

[49]A. Ivanov et al., "The binp road map for development of fusion reactor based on a linear machine", AIP Conference Proceedings **1771**, 080001 (2016).

[50]H. Hopf, "Abbildungsklassenn-dimensionaler mannigfaltigkeiten", Mathematische Annalen **96**, 209–224 (1927).

[51]M. Hazewinkel, "Poincaré–Hopf theorem", in *Encyclopedia of mathematics* (Kluwer Academic Publishers, 2001).

[52]I. Tamm, "Theory of a magnetic thermonuclear reactor (Part I)", in Plasma physics and the problem of controlled thermonuclear reactions, volume 1, edited by M. A. Leontovich (1961), p. 1.

[53]A. H. Boozer, "Plasma equilibrium with rational magnetic surfaces", The Physics of Fluids **24**, 1999–2003 (1981).

[54]D. A. Garren and A. H. Boozer, "Existence of quasihelically symmetric stellarators", Physics of Fluids B: Plasma Physics **3**, 2822–2834 (1991).

[55]A. H. Boozer, "Transport and isomorphic equilibria", The Physics of Fluids **26**, 496–499 (1983).

[56]M. Landreman and P. J. Catto, "Omnigenity as generalized quasisymmetry", Physics of Plasmas **19**, 056103 (2012).

[57]J. Freidberg, *Ideal mhd*, Ideal MHD (Cambridge University Press, 2014).

[58]J. Gibbs, *Elementary principles in statistical mechanics: developed with especial reference to the rational foundations of thermodynamics* (C. Scribner's sons, 1902).

[59]C. Cercignani, V. Gerasimenko, and D. Petrina, *Many-particle dynamics and kinetic equations*, Mathematics and Its Applications (Springer Netherlands, 1997).

[60]O. Embréus, "Kinetic modelling of runaway in plasmas" (Chalmers University of Technology, 2016).

[61]P. Helander and D. J. Sigmar, *Collisional transport in magnetized plasmas*, Cambridge Monographs on Plasma Physics (Cambridge University Press, 2005).

[62]S. Chapman et al., *The mathematical theory of non-uniform gases: an account of the kinetic theory of viscosity, thermal conduction and diffusion in gases*, Cambridge Mathematical Library (Cambridge University Press, 1990).

[63]S. Braginskii, "Transport Processes in a Plasma", Reviews of Plasma Physics **1**, 205 (1965).

[64]F. L. Hinton and S. K. Wong, "Neoclassical ion transport in rotating axisymmetric plasmas", The Physics of Fluids **28**, 3082–3098 (1985).

[65]I. G. Abel et al., "Multiscale gyrokinetics for rotating tokamak plasmas: fluctuations, transport and energy flows", Reports on Progress in Physics **76**, 116201 (2013).

[66]R. D. Hazeltine, "Recursive derivation of drift-kinetic equation", Plasma Physics **15**, 77 (1973).

[67]A. N. Simakov and P. J. Catto, "Drift kinetic equation exact through second order in gyroradius expansion", Physics of Plasmas **12**, 012105 (2005).

[68]R. D. Hazeltine, "Rotation of a toroidally confined, collisional plasma", The Physics of Fluids **17**, 961–968 (1974).

[69]I. Calvo et al., "Stellarator impurity flux driven by electric fields tangent to magnetic surfaces", Nuclear Fusion **58**, 124005 (2018).

[70]F. L. Hinton and R. D. Hazeltine, "Theory of plasma transport in toroidal confinement systems", Rev. Mod. Phys. **48**, 239–308 (1976).

[71]G. Kagan and P. J. Catto, "Arbitrary poloidal gyroradius effects in tokamak pedestals and transport barriers", Plasma Physics and Controlled Fusion **50**, 085010 (2008).

[72]M. Landreman et al., "Radially global δf computation of neoclassical phenomena in a tokamak pedestal", Plasma Physics and Controlled Fusion **56**, 045005, 045005 (2014).

[73]T. Pütterich et al., "Poloidal asymmetry of parallel rotation measured in ASDEX Upgrade", Nuclear Fusion **52**, 083013 (2012).

[74]I. Pusztai and P. J. Catto, "Neoclassical plateau regime transport in a tokamak pedestal", Plasma Physics and Controlled Fusion **52**, 075016 (2010).

[75]P. J. Catto et al., "A unified treatment of kinetic effects in a tokamak pedestal", Plasma Physics and Controlled Fusion **53**, 054004 (2011).

[76]G. Kagan et al., "Neoclassical theory of pedestal flows and comparison with Alcator C-Mod measurements", Contributions to Plasma Physics **52**, 365–371 (2012).

[77]P. J. Catto et al., "Kinetic effects on a tokamak pedestal ion flow, ion heat transport and bootstrap current", Plasma Physics and Controlled Fusion **55**, 045009 (2013).

[78]M. Landreman and D. R. Ernst, "Local and global Fokker–Planck neoclassical calculations showing flow and bootstrap current modification in a pedestal", Plasma Physics and Controlled Fusion **54**, 115006 (2012).

[79]P. W. Terry, "Suppression of turbulence and transport by sheared flow", Rev. Mod. Phys. **72**, 109–165 (2000).

[80]Y. Sarazin et al., "Large scale dynamics in flux driven gyrokinetic turbulence", Nuclear Fusion **50**, 054004 (2010).

[81]D. Told, "Gyrokinetic microturbulence in transport barriers" (Universität Ulm, 2012).

[82]S. Balay et al., *PETSc users manual*, tech. rep. ANL-95/11 - Revision 3.6 (Argonne National Laboratory, 2015).

[83]J. B. Taylor, "Diffusion of plasma ions across a magnetic field", The Physics of Fluids **4**, 1142–1145 (1961).

[84]R. D. Hazeltine and A. A. Ware, "Effects of electrostatic trapping on neoclassical transport in an impure plasma", The Physics of Fluids **19**, 1163–1176 (1976).

[85]C. Chang and R. Hazeltine, "Impurity transport in the collisional regime for large poloidal variations", Nuclear Fusion **20**, 1397–1405 (1980).

[86]C. Angioni and P. Helander, "Neoclassical transport of heavy impurities with poloidally asymmetric density distribution in tokamaks", Plasma Physics and Controlled Fusion **56**, 124001 (2014).

[87]C. Chang and R. Harvey, "Generation of poloidal electric field in a neutral-beam heated tokamak", Nuclear Fusion **23**, 935–939 (1983).

[88]S. Buller et al., "Collisional transport of impurities with flux-surface varying density in stellarators", Journal of Plasma Physics **84**, 905840409 (2018).

[89]P. Helander, F. I. Parra, and S. L. Newton, "Stellarator bootstrap current and plasma flow velocity at low collisionality", Journal of Plasma Physics **83**, 905830206 (2017).

[90]S. L. Newton et al., "Impurity transport and bulk ion flow in a mixed collisionality stellarator plasma", Journal of Plasma Physics **83**, 905830505 (2017).

[91]M. Landreman et al., "Comparison of particle trajectories and collision operators for collisional transport in nonaxisymmetric plasmas", Physics of Plasmas **21**, 042503, 042503 (2014).

[92]A. Mollén et al., "Impurities in a non-axisymmetric plasma: transport and effect on bootstrap current", Physics of Plasmas **22**, 112508 (2015).

[93]B. Geiger et al., "Observation of anomalous impurity transport during low-density experiments in W7-X with laser blow-off injections of iron", Nuclear Fusion **59**, 046009 (2019).

[94]F. Romanelli and JET EFDA Contributors, "Overview of the JET results with the ITER-like wall", Nuclear Fusion **53**, 104002 (2013).

[95]M. N. A. Beurskens et al., "The effect of a metal wall on confinement in JET and ASDEX upgrade", Plasma Physics and Controlled Fusion **55**, 124043 (2013).

[96]M. Beurskens et al., "Global and pedestal confinement in JET with a Be/W metallic wall", Nuclear Fusion **54**, 043001 (2014).

[97]C. Giroud et al., "Impact of nitrogen seeding on confinement and power load control of a high-triangularity JET ELMy H-mode plasma with a metal wall", Nuclear Fusion **53**, 113025 (2013).

[98]C. Maggi et al., "Pedestal confinement and stability in JET-ILW ELMy H-modes", Nuclear Fusion **55**, 113031 (2015).

[99]P. Snyder et al., "A first-principles predictive model of the pedestal height and width: development, testing and ITER optimization with the EPED model", Nuclear Fusion **51**, 103016 (2011).

[100]P. B. Snyder et al., "The EPED pedestal model and edge localized mode-suppressed regimes: studies of quiescent H-mode and development of a model for edge localized mode suppression via resonant magnetic perturbations", Physics of Plasmas **19**, 056115 (2012) http://dx.doi.org/10.1063/1.3699623.

[101]L. Frassinetti et al., "Global and pedestal confinement and pedestal structure in dimensionless collisionality scans of low-triangularity H-mode plasmas in JET-ILW", Nuclear Fusion **57**, 016012 (2017).

[102]S. R. Haskey et al., "Measurement of deuterium density profiles in the H-mode steep gradient region using charge exchange recombination spectroscopy on DIII-D", Review of Scientific Instruments **87**, 11E553, 11E553 (2016).

[103]E. Viezzer et al., "Collisionality dependence of edge rotation and in–out impurity asymmetries in ASDEX Upgrade H-mode plasmas", Nuclear Fusion **55**, 123002 (2015).

[104]E. Wolfrum et al., "Overview of recent pedestal studies at ASDEX Upgrade", Nuclear Fusion **55**, 053017 (2015).

[105]M. Bessenrodt-Weberpals et al., "The isotope effect in ASDEX", Nuclear Fusion **33**, 1205 (1993).

[106]S. D. Scott et al., "Isotopic scaling of confinement in deuterium-tritium plasmas", Physics of Plasmas **2**, 2299–2307 (1995).

[107]R. J. Hawryluk, "Results from deuterium-tritium tokamak confinement experiments", Rev. Mod. Phys. **70**, 537–587 (1998).

[108]J. Jacquinot and the JET team, "Deuterium-tritium operation in magnetic confinement experiments: results and underlying physics", Plasma Physics and Controlled Fusion **41**, A13 (1999).

[109]G. Manfredi and M. Ottaviani, "Gyro-bohm scaling of ion thermal transport from global numerical simulations of ion-temperature-gradient-driven turbulence", Phys. Rev. Lett. **79**, 4190–4193 (1997).

[110]D. Schissel et al., "Energy confinement properties of H-mode discharges in the DIII-D tokamak", Nuclear Fusion **29**, 185 (1989).

[111]J. Jacquinot and the JET team, "Deuterium-tritium operation in magnetic confinement experiments: results and underlying physics", Plasma Physics and Controlled Fusion **41**, A13 (1999).

[112]S. Braun and P. Helander, "Pfirsch-Schlüter impurity transport in stellarators", Physics of Plasmas **17**, 072514 (2010).

[113]P. Helander et al., "Impurity transport in a mixed-collisionality stellarator plasma", Phys. Rev. Lett. **118**, 155002 (2017).

[114]C. Beidler et al., "Benchmarking of the mono-energetic transport coefficients—results from the international collaboration on neoclassical transport in stellarators (ICNTS)", Nuclear Fusion **51**, 076001 (2011).

[115]S. Newton and P. Helander, "Neoclassical momentum transport in an impure rotating tokamak plasma", Physics of Plasmas **13**, 012505 (2006).

[116]A. Langenberg et al., "Impurity transport studies at Wendelstein 7-X by means of x-ray imaging spectrometer measurements", Plasma Physics and Controlled Fusion **61**, 014030 (2018).

[117]M. Hirsch et al., "Major results from the stellarator Wendelstein 7-AS", Plasma Physics and Controlled Fusion **50**, 053001 (2008).

[118]D. R. Mikkelsen et al., "Quasilinear carbon transport in an impurity hole plasma in LHD", Physics of Plasmas **21**, 082302 (2014).

[119]P. Helander and A. Zocco, "Quasilinear particle transport from gyrokinetic instabilities in general magnetic geometry", Plasma Physics and Controlled Fusion **60**, 084006 (2018).

[120]D. Hatch et al., "Direct gyrokinetic comparison of pedestal transport in JET with carbon and ITER-like walls", arXiv preprint arXiv:1903.02627 (2019).

[121]Y. Nakamura et al., "Impurity shielding criteria for steady state hydrogen plasmas in the LHD, a heliotron-type device", Plasma Physics and Controlled Fusion **56**, 075014 (2014).

[122]D. C. van Vugt et al., "Kinetic modeling of ELM-induced tungsten transport in a tokamak plasma", Physics of Plasmas **26**, 042508 (2019).